Dispersive Transport and Negative Bias Temperature Instability: Boundary Conditions, Initial Conditions, and Transport Models

Tibor Grasser, *Senior Member, IEEE*, Wolfgang Gös, and Ben Kaczer

(Invited Paper)

Abstract—**Negative bias temperature instability (NBTI) has evolved into one of the most serious reliability concerns for highly scaled pMOSFETs. It is most commonly interpreted by some form of reaction–diffusion model, which assumes that some hydrogen species is first released from previously passivated interface defects and then diffuses into the oxide. It has been argued, however, that hydrogen motion in the oxide is trap-controlled, resulting in dispersive transport behavior. This defect-controlled transport modifies the characteristic exponent in the power law that describes the threshold-voltage shift. So far, a number of NBTI models based on dispersive transport have been published. Interestingly, although seemingly based on similar physical assumptions, these models result in different predictions. Most notably, both an increase and a decrease in the power-law time exponent with increasing dispersion have been reported. Also, different functional dependences on the dispersion parameter have been given in addition to differences in the prefactors and the saturation behavior. We clarify these discrepancies by identifying the boundary and initial conditions which couple the transport equations to the electro-chemical reaction at the interface as the crucial component. We proceed by deriving a generalized reaction (dispersive) diffusion formalism and provide the missing link between the various published models by demonstrating how each of them can be derived from this generalized model.**

Index Terms—**Analytical models boundary condition, bias temperature instability, dispersive transport, initial condition, negative bias temperature instability (NBTI), numerical solution, power law, stretched-exponential.**

I. INTRODUCTION

AMONG the various reliability issues in modern CMOS technology, negative bias temperature instability (NBTI) has been identified as one of the most serious concerns for highly scaled pMOSFETs [1]–[4]. Most commonly, models based on the reaction–diffusion (RD) theory originally proposed by Jeppson and Svensson 30 years ago [5], [6] are used to explain NBTI. Recently, a lot of effort has been put into refining the classic RD theory [2], [7], [8]. The RD model assumes that Si–H bonds at the semiconductor–oxide interface are broken at higher temperatures and electric fields, causing the released hydrogen species to diffuse into the oxide. As a result, one obtains the change in the silicon dangling bond density $\Delta N_{\rm it} = [{\rm Si}^\bullet] - [{\rm Si}^\bullet]_0$ at the interface, with $[{\rm Si}^\bullet]_0$ as the initial density of dangling bonds. It can be shown [2] that the RD model gives a fractional power law for the evolution of $\Delta N_{\rm it}$

$$\Delta N_{\rm it}(t) = A(T, E_{\rm ox})t^n. \tag{1}$$

In the RD framework, H_2 is often assumed as a diffusing species because it gives a characteristic time exponent of $n = 1/6$ for the threshold-voltage shift, which is consistent with some [8], [9], but not all [10], recent delay-free measurements, whereas H^0 and H^+ result in $n = 1/4$ and $n = 1/2$, respectively [7].

From $\Delta N_{\rm it}$, the threshold-voltage shift is normally estimated by assuming that all traps are positively charged, that is, $\Delta Q_{\rm it}(E_F) \approx q\Delta N_{\rm it}$, which is an assumption that is only actually fulfilled during a strong negative bias where the Fermi-level at the semiconductor–oxide interface is close to the valence band edge [11]. In fact, for a proper consideration of the Fermi-level dependence, the accurate trap density-of-states has to be known [12]. This is particularly important for the understanding of measurement results, be that an $I_D V_G$ characteristic, charge-pumping, or DCIV measurements, where the Fermi-level is moved to completely different energies.

In addition to interface state generation, which seems to be the universally acknowledged feature of NBTI [1], [4], positive charge generation in the oxide bulk has been reported [11], [13], [14]. Positive charge has been attributed to trapped holes either in preexisting traps [13], [14] or in traps generated by the released hydrogen species [11]. Independent of the controversial question whether the contribution of trapped charges is important or not [3], [15], we focus here on hydrogen transport and the interaction of hydrogen with dangling bonds at the interface, which is the ingredient of most NBTI models. The contribution of oxide charges and the trap occupancy have to be added on top of the contribution by a separate model, if required.

During the last couple of years, several alternative explanations to the classic RD model have been put forward [3], [11], [16]–[18]. In particular, it has been argued that transport of the hydrogen species inside the oxide is dispersive [2], [11], [16], [17], which is consistent with hydrogen diffusion measurements [19], [20] and available models for irradiation damage [21], [22]. Interestingly, in these models, the power-law exponent depends on a temperature-dependent dispersion parameter. Another feature is that the trap density-of-states directly influences the dispersion parameter and thus the exponent and the magnitude of the observed threshold-voltage shift, which makes it possible to incorporate technology-dependent behavior into the model. As another consequence, these models brought H^+ back into the game, which had originally been dismissed due to the 1/2 exponent resulting from the RD model.

One feature common to published trap-controlled dispersive NBTI models is that they predict a reduction of the power-law exponent with increasing dispersion [11], [16], [17]. However, in contrast to that, it was observed that inclusion of traps into the standard RD model increases the exponent [7]. In addition, our own simulations showed [12] that a straightforward application of the dispersive multiple-trapping (MT) transport model [23]–[25] also increases the exponent, which is in contradiction to these published reaction-dispersive-diffusion (RDD) models [2], [11], [16], [17]. A detailed analysis reveals that the boundary condition at the Si/SiO$_2$ interface is the main reason for this discrepancy. It is shown that the choice of boundary condition is essential for the overall behavior of the dispersive system.

Another interesting issue in that context is the fact that the dispersive proton transport models proposed by Kaczer *et al.* [17] and Zafar [11] show a different dependence of the power-law exponent on the dispersion parameter α. While the Kaczer–Arkhipov model gives $n = \alpha/2$, the Zafar model arrives at $n = \alpha$. Also, the prefactor in the Kaczer–Arkhipov model depends on the square-root of the diffusivity, whereas the Zafar model predicts a linear dependence. The latter is insofar of relevance as the linear dependence of ΔN_{it} on the diffusivity has been used by Zafar to explain the isotope effect [4], [11].

Thus, the question related to the origin of these discrepancies arises. In order to understand this issue, the differences and similarities in the physical assumptions invoked during the derivation of both models are investigated. An important issue in that context is the fact that models based on the classic RD theory assume that all interface traps contribute equally to the threshold-voltage shift. In the model of Zafar [11], however, a different interpretation is introduced by assuming that a large number of dangling bonds always exist but only a fraction can be observed in electrical measurements, whereas the majority is too close to the band edges to contribute. During NBT stress, the total number of interface states is increased, and only this increase is visible during measurements. To model this partial contribution of the generated interface states to the observable threshold-voltage shift, the occupancy of the interface states as a function of the Fermi-level position has to be introduced [11], [12].

Zafar derived her model using statistical mechanics, without explicitly stating the electro-chemical reaction at the interface, which is equivalent from a mathematical point of view. We also demonstrate how the assumptions introduced by Zafar can be incorporated into generalized RD and RDD models. For the sake of completeness, we note that the threshold-voltage shift in the final Zafar model is attributed to a contribution of chargeable interface states and oxide defects. However, both contributions are directly calculated from the shift in ΔN_{it} by using two different occupancy probabilities for oxide and interface states. Thus, we can limit our discussion to the underlying transport problem and the corresponding initial and boundary conditions.

A fundamental problem during the study of NBTI is related to the fact that the damage created during the stress phase begins to relax immediately once the stress is removed. This makes the classic measurement technique problematic, where the stress is interrupted during the extraction of the threshold voltage [26], [27]. In particular, the value of the extracted power-law exponent depends significantly on the delay introduced during the measurement [28]. Experimental results obtained with delayed measurements show a linear increase of the exponent with temperature [3], [17], with the exponent being around 0.2–0.3. In contrast, temperature-independent exponents in the range 0.1–0.2 have been extracted from delay-free measurements [9], [29]. Provided that the generation of interface defects is the only mechanism responsible for NBTI, one may expect the model to predict a temperature-independent exponent in a delay-free setup. On the other hand, it is just as reasonable to require the model to predict this linear dependence of the slope in delayed measurements. We remark that none of the existing models can currently satisfy both requirements [30].

On the other hand, if an additional effect on top of interface state generation occurs, like hole-trapping [3], [27], [31], the interpretation is more involved [30]. Assuming that this additional mechanism results in a temperature-independent exponent, it might dominate the temperature-independent exponent during delay-free measurements, whereas during delayed measurements, fast recovery of this additional process may expose the underlying interface state creation mechanism, which might then show the observed temperature dependence. For this assumption to hold, the additional component must be large enough to overshadow any temperature dependence of the interface state creation mechanism.

In the following, we will derive a generalized RD formalism suitable for our purposes. Since RDD models will be considered as extensions of the standard RD theory, its foundations will be revisited in some detail first. Thereby, care is taken in formulating the results in such a way that they can be directly transferred to the dispersive transport case where particular attention will be paid to potential pitfalls. This generalized formalism allows us to identify the differences and similarities existing in the various published models. As such, the main purpose of this paper is not the derivation of a new model for NBTI degradation but rather the derivation of a unified modeling framework that allows us to pin-down the differences observed in the existing models.

II. GENERALIZED RD FORMALISM

The RD model consists basically of an electro-chemical reaction at the semiconductor–oxide interface, which is coupled to a drift-diffusion equation in the oxide bulk. Without considering the questions whether the depassivation process is field-driven [2], [32], why holes at the interface are required and how they influence the reaction [18], and in which charge state (neutral or positive) the created trap and the released hydrogen species are, we write

$$\text{Si} - \text{H} \rightleftharpoons \text{Si}^\bullet + \text{H}_c + \text{H}_t. \tag{2}$$
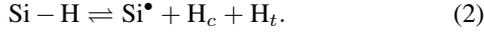
Thereby, we differentiate between hydrogen in a conduction/mobile state H_c and trapped hydrogen H_t [33]. We will show in Section IV that this distinction is important since in dispersive transport models most hydrogen becomes trapped quickly and might not be available for the reverse reaction. We also note that a large background concentration of hydrogen may exist in the vicinity of the interface, possibly in the order of 10^{19} cm^{-3} [34], which, if assumed to be freely available, could dominate the reverse reaction and completely compensate the forward reaction in a standard RD model.

It has been claimed that the binding energies of the Si–H bonds display a Gaussian broadening [3], [35]. Previously published dispersive NBTI models consider either a dispersion in the forward rate [3] or a dispersion in the transport properties [11], [16], [17], but not both. Although both options are feasible, we focus in this paper on dispersive transport only. In particular, the variations in the energy barrier for the reverse reaction become important in the context of dispersive transport.

In the standard RD formulation, the barrier is considered to be single valued, and $H_t = 0$. The kinetic equation describing the interface reaction is commonly assumed to be of the form [6], [36], [37]

$$\frac{\partial N_{\text{it}}}{\partial t} = k_f(N_0 - N_{\text{it}}) - k_r N_{\text{it}} H_{\text{it}}^{1/a} \tag{3}$$

where $N_{\text{it}} = [\text{Si}^\bullet]$ is the interface state density, $N_0 = [\text{Si–H}]_0$ is the initial density of passivated interface defects, H_{it} is the hydrogen concentration at the semiconductor–oxide interface, and k_f and k_r are the temperature- and possibly field-dependent rate coefficients, while a gives the order of the reaction (one for H^0 and H$^+$, and two for H$_2$, assuming an instantaneous conversion of H^0 to H$_2$, cf., [37]). In our context, it is important to recall that the usual assumptions are that $N_{\text{it0}} = N_{\text{it}}(0) = 0$ at the beginning of the stress period and that all generated N_{it} contribute equally to the threshold-voltage shift. A somewhat surprising feature of the RD equations is, as will be shown in the following, that, by allowing a larger number of initial interface defects, a completely different behavior is obtained.

Hydrogen motion is assumed to be controlled by conventional drift-diffusion [6]

$$\frac{\partial H_c}{\partial t} = -\nabla \cdot \mathcal{F} H_c + G_c \tag{4}$$

$$\mathcal{F} = -D_c \left(\nabla - Z \frac{\mathbf{E}_{\text{ox}}}{V_T} \right) \tag{5}$$

with $H_c(\mathbf{x}, 0) = 0$. Hydrogen transport is postulated to occur on a single energy level, which will be referred to as the conduction state, with H_c, D_c, and G_c as the hydrogen concentration, diffusivity, and generation rate in the conduction state, respectively, $\mathcal{F}$ as the flux operator, Z as the charge state of the particle, $V_T = k_B T_L/\text{q}$ as the thermal voltage, T_L as the lattice temperature, and $\mathbf{E}_{\text{ox}}$ as the electric field inside the oxide.

The generation rate G_c is given by the interface reaction and reads for the usually considered 1-D problem

$$G_c(\mathbf{x}, t) = G_0(t)\delta(x - x_0) \tag{6}$$

$$G_0(t) = \frac{1}{a}\frac{\partial N_{\text{it}}}{\partial t}. \tag{7}$$

Alternatively, one may introduce an influx of newly created species at the boundary by integrating (4) over an infinitesimally thin interfacial layer. This results in

$$\mathcal{F} H_c|_{\text{it}} \cdot \mathbf{n} = G_0 \tag{8}$$

with $\mathbf{n}$ as the normal vector at the interface. Although (8) is the conventionally employed formalism, we will also use the spatial generation rate (6) as it can be more intuitively extended to dispersive transport models.

For the calculation of the time-dependent density of interface states N_{it}, (3) and (4) can be solved numerically on an arbitrary geometry. However, for some special cases, analytical approximations can be given [37]–[39], which are helpful in understanding the basic kinetics. Although the solution of the RD model depends on the underlying geometry [40], it is commonly assumed that NBTI is a 1-D problem. For the sake of conciseness, we will derive our analytical models for a 1-D geometry.

Depending on the parameter values and boundary conditions, different phases are observed, which are shown in Fig. 1 for the three most commonly used species: H$^+$, H^0, and H$_2$. 1) The reaction-dominated regime with an exponent $n = 1$, where the reverse rate is negligible due to the lack of available H_{it}; 2) Depending on the parameter values, a transition regime where $\partial N_{\text{it}}/\partial t = 0$, which gives an exponent $n = 0$; 3) The quasi-equilibrium regime where $\partial N_{\text{it}}/\partial t$ is much smaller than the generation and passivation terms. This is assumed to be the dominant regime and displays the characteristic time exponent depending on the created species; and 4) A saturation regime which could be either a soft saturation due to a reflecting boundary condition or a hard saturation resulting from the depassivation of all passivated interface states [41]. As the nature and influence of the oxide-poly boundary is not yet resolved [8], [41], we will restrict our discussion to the case of an infinitely thick oxide, which is an issue of little consequence to the discussion presented here.[1] In contrast, the numerical results used for the model validation are obtained

---

[1]For instance, it has been reported that a change in the transport properties of hydrogen inside the oxide and the poly layer may result in an intermediate kink in the threshold voltage shift [8], [30], [42], which is an issue that is still to be confirmed experimentally. However, the fundamental kinetics would remain unchanged.
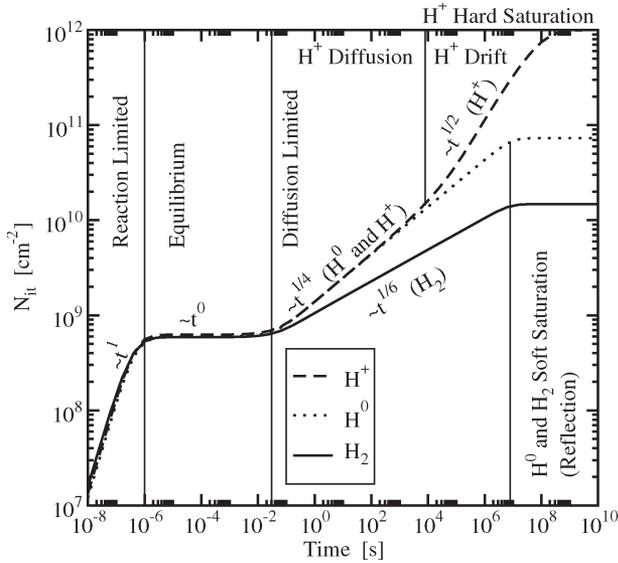
Fig. 1. Five phases of the standard RD model obtained from a numerical solution of (3) and (4) on a 2-nm oxide, using the parameters $N_0 = 10^{12}$ cm^{-2} and $N_{it0} = 0$. Shown are the results for the three species H$^+$, H^0, and H$_2$. The time exponent $n = 1$ is the signature of the reaction-limited phase, whereas $n = 1/4, \ldots, 1/2$, $n = 1/4$, and $n = 1/6$ are observed for the three species in the diffusion-limited phase. At the beginning of the diffusion-limited phase, H$^+$ behaves like H^0. Furthermore, in the nonselfconsistent simulation, where the feedback of the charges on the field distribution is neglected, H$^+$ does not show a soft saturation since all hydrogen is pulled away from the interface.

by using a perfectly reflecting boundary condition on a 2-nm oxide. As such, the analytical approximations give the correct initial trends but do not account for saturation or other effects induced by the oxide-poly boundary.

The RD model assumes the quasi-equilibrium of the interface reaction $(\partial N_{it}/\partial t \approx 0)$ to be the dominant regime [2], [11], [17]. Consequently, we obtain from (3)

$$\left(\frac{k_f}{k_r} \frac{N_0 - N_{it}}{N_{it}} \right)^a = H_{it}. \tag{9}$$

The RHS of (9) contains the interfacial hydrogen concentration which, at least in principle, has to be determined by solving the coupled drift-diffusion equation in the bulk. Two identities are helpful in that context. The first one is obtained by integrating the continuity equation (4) over time and the positive half-space

$$\Delta N_{it}(t) = a \int_0^\infty H_c(x,t) dx \tag{10}$$

with $\Delta N_{it}(t) = N_{it}(t) - N_{it0}$. We now introduce a general parameter $B(t)$ as

$$\int_0^\infty H_c(x,t) dx \equiv B(t) H_{it}(t) \tag{11}$$

which depends on the transport model and the geometry. This allows us to express H_{it} as

$$H_{it}(t) = \frac{\Delta N_{it}(t)}{a B(t)}. \tag{12}$$

Alternatively, we can reformulate the boundary condition (8) by introducing a time-dependent parameter $C(t)$ as

$$\mathcal{F} H_c(t)|_{it} \cdot \mathbf{n} \equiv C(t) H_{it}(t) \tag{13}$$

and consequently write

$$H_{it}(t) = \frac{G_0(t)}{C(t)} = \frac{1}{aC(t)} \frac{\partial N_{it}}{\partial t}. \tag{14}$$

Provided the exact hydrogen profile $H_c(\mathbf{x}, t)$ is known, (12) and (14) are equivalent. However, since in the analytical approximations a guess for $H_c(\mathbf{x}, t)$ is used, these two formulations lead to slightly different results.

In order to bypass the complete solution of the coupled drift-diffusion equation [6], which results in rather complex analytical expressions for $H_c(\mathbf{x}, t)$, for many purposes, approximate solutions have been proven to be useful. Alam suggested [2], [37], [38] to use a triangular hydrogen profile (on a lin–lin scale) of the width $\sqrt{D_c t}$ for neutral species. A more rigorous but closely related expression can be derived from the complementary error function diffusion profile, which results from a constant surface concentration. This is not quite the case for NBTI where the assumption of a constant surface concentration holds only during the initial stress phase and is later replaced by a constant dose criterion during the saturation phase, which would then result in a Gaussian profile [43]. Nevertheless, expressions of the form

$$B(t) = \lambda_0 \sqrt{D_c t} \tag{15}$$

$$C(t) = \Lambda_0 \sqrt{D_c/t} \tag{16}$$

are reasonably accurate before the onset of saturation, with $\lambda_0 = 1/2$ and $\Lambda_0 = 1$ for the linear profile, and $\lambda_0 = 2/\sqrt{\pi}$ and $\Lambda_0 = 1/\sqrt{\pi}$ for the complementary error function. In addition, λ_0 and Λ_0 can be adjusted empirically [37]. However, the improved accuracy is of little practical relevance during the presaturation stress phase. An interesting feature is the fact that for diffusing species $(Z = 0)$, area estimation (15) is more accurate than flux estimation (16) and thus preferable. In other words, it is easier to get the area of a diffusion-dominated profile right than the gradient straight at the interface.

Analogously, for the proton, it is assumed that the drift-term dominates. By approximating the hydrogen profile by a rectangle [42] of width $v_c t = \mu_c E_{ox} t$, one obtains

$$B(t) = \mu_c E_{ox} t \tag{17}$$

$$C(t) = \mu_c E_{ox}. \tag{18}$$

The mobility is assumed to be related to the diffusivity [4] via the Einstein relation as $\mu_c = D_c/V_T$. Contrary to the diffusing species where the area estimation is more accurate, for pure drift, flux estimation (18) gives results closer to the full numerical solution and should thus be preferred over area estimation (17).

Quite generally, for any species and transport model considered here, we will introduce

$$B(t) = B_0 t^b \tag{19}$$

$$C(t) = C_0 t^{c-1}. \tag{20}$$

TABLE I
HYDROGEN PROFILE SHAPE FUNCTIONS FOR THE THREE
TRANSPORT MODELS CONSIDERED IN THIS PAPER

	H^+	H^0 (H_2)
a	1	1 (2)
Drift-Diffusion		
B	$D_c \dfrac{E_{ox}}{V_T} t$	$\lambda_0 \sqrt{D_c t}$
B_0	$D_c \dfrac{E_{ox}}{V_T}$	$\lambda_0 \sqrt{D_c}$
b	1	1/2
C	$D_c \dfrac{E_{ox}}{V_T}$	$\Lambda_0 \sqrt{D_c/t}$
C_0	$D_c \dfrac{E_{ox}}{V_T}$	$\Lambda_0 \sqrt{D_c}$
c	1	1/2
Multiple-Trapping Drift-Diffusion		
B	$\dfrac{D_c}{\nu}\dfrac{N_c}{N_t}\dfrac{E_{ox}}{V_T}(\nu t)^\alpha$	$\left(\dfrac{D_c}{\nu}\dfrac{N_c}{N_t}\right)^{1/2}(\nu t)^{\alpha/2}$
B_0	$\dfrac{D_c}{\nu}\dfrac{N_c}{N_t}\dfrac{E_{ox}}{V_T}\nu^\alpha$	$\left(\dfrac{D_c}{\nu}\dfrac{N_c}{N_t}\right)^{1/2}\nu^{\alpha/2}$
b	α	$\alpha/2$
Phenomenological Drift-Diffusion		
B	$\dfrac{D_{00}}{\nu_0}\dfrac{E_{ox}}{V_T}(\nu_0 t)^\beta$	$\lambda_0\left(\dfrac{D_{00}}{\nu_0}\right)^{1/2}(\nu_0 t)^{\beta/2}$
B_0	$\dfrac{D_{00}}{\nu_0}\dfrac{E_{ox}}{V_T}\nu_0^\beta$	$\lambda_0\left(\dfrac{D_{00}}{\nu_0}\right)^{1/2}\nu_0^{\beta/2}$
b	β	$\beta/2$
C	$D_{00}\dfrac{E_{ox}}{V_T}(\nu_0 t)^{\beta-1}$	$\Lambda_0\left(\dfrac{D_{00}}{\nu_0}\right)^{1/2}\nu_0^{\beta/2}t^{\beta/2-1}$
C_0	$\dfrac{D_{00}}{\nu_0}\dfrac{E_{ox}}{V_T}\nu_0^\beta$	$\Lambda_0\left(\dfrac{D_{00}}{\nu_0}\right)^{1/2}\nu_0^{\beta/2}$
c	β	$\beta/2$

We note that, for the approximations discussed in this paper, $b = c$ holds. As will become clear later, the main advantage of introducing (19) and (20) is that it allows us to formulate the final NBTI models independently of the species, transport model, and, under certain circumstances, the assumed boundary conditions. The parameter values for the various models discussed in this paper are summarized in Table I.

After having established the area and flux formulations (12) and (14), we obtain two fundamental RD equations. First, by inserting (12) into (9), one obtains the area formulation

$$\left(\frac{k_f}{k_r}\frac{\Delta N_{it,max} - \Delta N_{it}}{N_{it0} + \Delta N_{it}}\right)^a = \frac{\Delta N_{it}}{aB} \qquad (21)$$

or, alternatively, using (14) with (9) gives the flux formulation

$$\left(\frac{k_f}{k_r}\frac{\Delta N_{it,max} - \Delta N_{it}}{N_{it0} + \Delta N_{it}}\right)^a = \frac{1}{aC}\frac{\partial \Delta N_{it}}{\partial t} \qquad (22)$$

with the maximum value of ΔN_{it} given by $\Delta N_{it,max} = N_0 - N_{it0}$.

We repeat that, provided the expressions for B and C are accurate, (21) and (22) will deliver the same result. Using, for instance, the approximate relationships (15) and (16), however,

will give different results, most notably because (21) is an algebraic equation in ΔN_{it} whereas (22) is a first-order differential equation in time. As will be shown later, both expressions result in a practically time-independent offset to the correct solution during the presaturation phase. This offset is of little practical importance as hardly any parameter of the RD model is known with any certainty anyway. However, in the saturation regime, (21) results in a square-root-like behavior, whereas (22) might be best approximated by a stretched-exponential.

Equations (21) and (22) are straightforward to solve for ΔN_{it}. Unfortunately, (21) gives a rather lengthy result [see (30) for the proton case], whereas (22) only results in an implicit expression for ΔN_{it}, which might be approximated by a stretched-exponential. Both results have in common that, depending on the relative value of ΔN_{it} to N_{it0}, the solution behaves quite differently. The two asymptotic limits $\Delta N_{it} \ll N_{it0}$ and $\Delta N_{it} \gg N_{it0}$ are very intuitive and will be discussed in the following. Also, saturation is first neglected ($N_{it}(t) \ll N_0$) and discussed in Section II-D.

A. Small Concentration of Initial Interface States

With the assumption $\Delta N_{it}(t) \gg N_{it0}$, the standard RD model is obtained from (21)

$$\Delta N_{it}(t) = A_{RD}B^{1/(1+a)}(t) \qquad (23)$$

with the species-dependent prefactor

$$A_{RD} = \left(a\left(\frac{k_f}{k_r}\Delta N_{it,max}\right)^a\right)^{1/(1+a)}. \qquad (24)$$

In contrast, by using the flux formulation (22), one obtains

$$\Delta \tilde{N}_{it}(t) = \left(\frac{1+a}{c}\frac{C_0}{B_0}\right)^{1/(1+a)}\Delta N_{it}(t) \qquad (25)$$

which differs from (23) by a constant prefactor. With the complementary error function profile, this prefactor is equal to $\sqrt{2}$ and $3^{1/3}$ for H^0 and H_2, respectively, while the linear profile gives roughly twice these values. For the proton model, the prefactor of (25) is $\sqrt{2}$, which is precisely the result delivered by the dispersive drift models based on the MT model and is in excellent agreement with the numerical solution.

With the appropriate shape functions (17) and (15), (23) and (25) give the exponents $n = b/(1 + a)$, which are the well-known values of 1/2, 1/4, and 1/6 for proton, atomic, and molecular hydrogen transport, respectively. These exponents do not depend on temperature nor is it possible to include process dependences. Again, we note that the exponent of 1/2 obtained from the RD model for H^+ transport is not observed experimentally, which led researchers to discard this possibility. On the other hand, the exponent for molecular hydrogen diffusion ($n = 1/6$) is close to the values observed in recent delay-free measurements, ≈ 0.12–0.14 [9], [29], making some researchers favor that model [29], [44]. However, the issue of temperature-dependent delayed-slopes remains unanswered in the classic RD model [30].

B. Large Concentration of Initial Interface States

Interestingly, by assuming $\Delta N_{\text{it}}(t) \ll N_{\text{it0}}$, a completely different solution is obtained. This is because ΔN_{it} in the denominator on the LHS of (21) can be neglected against N_{it0}, which results in $\Delta N_{\text{it}}^{1/a}$ instead of $\Delta N_{\text{it}}^{1/a+1}$. In the area formulation (21), one obtains

$$\Delta N_{\text{it}}(t) = A_P B(t) \tag{26}$$

with the prefactor

$$A_P = a \left(\frac{k_f}{k_r} \frac{\Delta N_{\text{it,max}}}{N_{\text{it0}}} \right)^a = A_{\text{RD}}^{1+a} N_{\text{it0}}^{-a}. \tag{27}$$

Again, in contrast, flux formulation (22) gives

$$\Delta \tilde{N}_{\text{it}}(t) = \frac{1}{c} \frac{C_0}{B_0} \Delta N_{\text{it}}(t). \tag{28}$$

As before, (28) differs from (26) by a constant prefactor. Interestingly, for neutral diffusing species, the prefactor is equal to four, with the estimation based on the linear hydrogen profile, whereas the complementary error function profile results in exactly one. Also, there is no difference in the proton drift model. In this regime, the exponent obtained by the RD model is equal to $n = b$, with the values 1, 1/2, and 1/2 for proton, atomic, and molecular hydrogen transport, respectively. Note that the exponents are solely determined by the area function B rather than a combination of area function and kinetic exponent a as in the standard RD model. For classic drift-diffusion, these resulting exponents are not compatible with measurements. However, as will be shown in the following, the introduction of dispersive transport can bring the exponents within the observed ranges.

The assumption $\Delta N_{\text{it}}(t) \ll N_{\text{it0}}$ has originally been introduced by Zafar [11]. This is based on the (actually mandatory) notion that the occupancy of the interface states depends on the position of the Fermi-level and that not all interface states are electrically active. In this context, N_0 is now the maximum number of hydrogen binding sites rather than the maximum number of electrically observable interfaces states in a completely depassivated sample.

C. Intermediate Concentration of Initial Interface States

For an intermediate concentration of initial interface states, a transition between the two regimes given through (23) and (26) is observed. Since the condition $\Delta N_{\text{it}}(t) \ll N_{\text{it0}}$ will be valid during early times, the regime described by (26) will be labeled pre-RD in the following. One may define the transition point to the standard RD scheme as the time where $\Delta N_{\text{it}}(t) = N_{\text{it0}}$, and we obtain by inverting (26)

$$t_{\text{RD}} = \left(\frac{N_{\text{it0}}}{A_P B_0} \right)^{1/b}. \tag{29}$$

The time point given through (29) is also (roughly) equivalent to the intersection point of (23) and (26). Such a transition
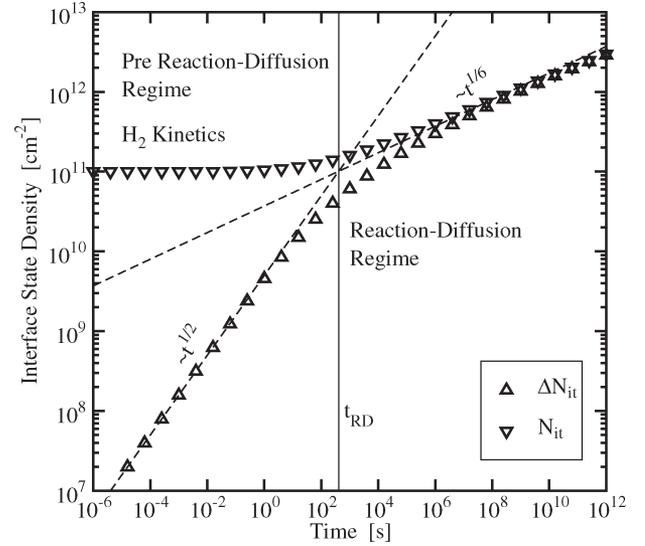

Fig. 2.   Two different regimes for a medium number of initial interface defects $N_{\text{it0}} = 10^{11}$ cm^{-2} given through (21). The transition between the pre-RD regime and the standard RD regime at $t = t_{\text{RD}}$ can be clearly observed. A value of $N_0 = 10^{13}$ cm^{-2} was used.

is depicted in Fig. 2 for the values $N_{\text{it0}} = 10^{11}$ cm^{-2} and $N_0 = 10^{13}$ cm^{-2}. Obviously, for $N_{\text{it0}} = 0$, we obtain $t_{\text{RD}} = 0$, that is, only the conventional RD regime is observed. However, for large N_{it0} closer to N_0, the transition occurs very late or not at all due to the onset of saturation.

D. Saturation

While the different expressions for H_{it} resulted only in a constant prefactor during the stress phase, inaccuracies in the estimation for H_{it} influence the saturation behavior more significantly. Although these differences are of minor practical importance, they explain the different expressions given in literature [11], [41], [45].

For the sake of brevity, we limit the following discussion to proton and atomic hydrogen transport ($a = 1$). We first solve the full RD equation in the area formulation (21), which has the solution

$$\Delta N_{\text{it}}(t) = \frac{K(t) + N_{\text{it0}}}{2} \left(\sqrt{1 + \frac{4K(t)\Delta N_{\text{it,max}}}{(K(t) + N_{\text{it0}})^2}} - 1 \right) \tag{30}$$

with $K(t) = B k_f/k_r$. While the expression in the RD regime for small N_{it0} is obvious, in the pre-RD regime with $\Delta N_{\text{it}} \ll N_{\text{it0}}$, we obtain by expanding the square-root for large N_{it0}

$$\Delta N_{\text{it}}(t) = \frac{\Delta N_{\text{it,max}}}{1 + (t/\tau_{\text{PL}})^{-b}} \tag{31}$$

with

$$\tau_{\text{PL}} = \left(\frac{N_{\text{it0}}}{B_0} \frac{k_r}{k_f} \right)^{1/b}. \tag{32}$$

Interestingly, based on a dispersion of the forward-rate k_f only, an expression of the form (31) has been derived by

Huard *et al.* [13] and successfully fitted to their measurement data. There, the exponent b depends on the variance of the distribution of forward rates and the temperature. Here, as will be shown later, the introduction of dispersive transport makes b dependent on the dispersion parameter of the transport equation and consequently also on the temperature.

In contrast, if we solve the flux-based expression (22), we obtain the general implicit solution

$$\frac{\Delta N_{\text{it}}}{N_0} + \log\left(1 - \frac{\Delta N_{\text{it}}}{\Delta N_{\text{it,max}}}\right) = -\left(\frac{t}{\tau_P}\right)^c \qquad (33)$$

where we introduced

$$\tau_P = \left(c\,\frac{k_r}{k_f}\,\frac{N_0}{C_0}\right)^{1/c}. \qquad (34)$$

In the RD regime, (33) can be approximated by a stretched-exponential [45]

$$\Delta N_{\text{it}}(t) = \Delta N_{\text{it,max}}\left(1 - \exp\left(-\left(\frac{t}{\tau_{\text{RD}}}\right)^{c/2}\right)\right) \qquad (35)$$

with $\tau_{\text{RD}} = \tau_P/2^{1/c}$. Note that for short times $t < \tau_{\text{RD}}$, the aforementioned expression has the correct asymptotic limit (25).

In contrast, when we assume that $\Delta N_{\text{it}} \ll N_0$ at all times [46], which is a much more stringent assumption than $\Delta N_{\text{it}} \ll N_{\text{it0}}$ used to differentiate the pre-RD from the RD regime, one can neglect the first term on the LHS of (33) to obtain the stretched-exponential given by Zafar for her dispersive-drift model [11]

$$\Delta N_{\text{it}}(t) = \Delta N_{\text{it,max}}\left(1 - \exp\left(-\left(\frac{t}{\tau_P}\right)^c\right)\right). \qquad (36)$$

Note the different exponent compared to (35) and the slightly different time constant. We remark that the condition $\Delta N_{\text{it}} \ll N_0$ at all times requires N_{it0} to be very close to N_0. Otherwise, the first term on the LHS of (33) cannot be neglected. This can also be seen from the Taylor expansion of the stretched-exponential (36), which gives

$$\Delta N_{\text{it}}(t) = \frac{N_{\text{it0}}}{N_0}\frac{1}{c}\frac{C_0}{B_0}A_P B(t). \qquad (37)$$

which differs from the exact solution (28) by the ratio N_{it0}/N_0. In contrast, an expansion of the (implicit) full solution (33) correctly results in (28). Thus, the error in the stretched-exponential is only small for $N_{\text{it0}} \approx N_0$. In particular, for the stretched-exponential to be accurate in the most important stress phase within p percent, N_{it0} has to be larger than $N_0 \times p/100$. The accuracy of the power-law-like approximation (31), on the other hand, is not as sensitive to the value of N_{it0}, and it includes the correct short time limit of the implicit full solution (33). These results will be discussed in more detail in Section VI-B.
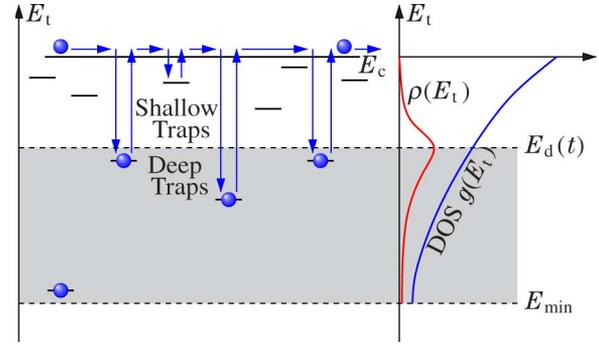

Fig. 3. Schematic illustration of dispersive transport. Particles in the hydrogen conduction band fall into the traps and are reemitted into the conduction band. Reemission is more likely for shallow traps. The time-dependent demarcation energy E_d separates shallow from deep traps. With time, the demarcation energy becomes more negative until the bottom of the trap distribution is reached ($E_d \to E_{\min}$) and equilibrium is obtained. As a result, the motion of the particle packet slows down with time. Note how the individual trap levels, which microscopically correspond to the different energy levels of hydrogen in an amorphous material, are approximated by a macroscopic density-of-states.

III. DISPERSIVE TRANSPORT

In contrast to drift-diffusion transport, dispersive transport is trap-controlled. This implies that most particles reside on trap levels. Depending on the trap level energy (the distance to the "conduction band"), hydrogen can easily be released from shallow traps but has large release times from deep traps. This is schematically illustrated in Fig. 3.

RDD models proposed so far have relied on simplified transport models developed either for the time evolution of an initial hydrogen profile after an irradiation pulse [16], [17], [21], [22] or on a phenomenological time-dependent diffusivity as observed in hydrogen diffusion and annealing experiments [2], [11], [19], [20]. The applicability of these simplified equations to the problem at hand has not been rigorously assessed and, as we will show in the following, contains the following pitfalls.

1) First, during NBTI stress, one has to deal with a continuous influx of particles which has to be properly accounted for in the boundary condition of the model equations.

2) Second, the reverse rate of the interface reaction depends on the concentration of available hydrogen at the interface. Here, one might have to consider that, in the dispersive case, most particles reside in deep traps rather than in the "conduction state." As will be shown, this issue is of fundamental importance to the model as it results in completely different time exponents.

A. MT Model

Dispersive transport is often described using the continuous time random walk (CTRW) theory [47] or MT models [23]–[25]. Both models exhibit similar features [48]–[50] and will be considered equivalent in the following [49]. Since the MT model lends itself exceptionally well to a numerical and analytical treatment and is easier to solve for arbitrary initial and boundary conditions, we use the MT equations in our discussions.

In the MT model, the total hydrogen concentration H consists of hydrogen in the conduction states H_c and trapped hydrogen as

$$H(\mathbf{x}, t) = H_c(\mathbf{x}, t) + \int \rho(\mathbf{x}, E_t, t) dE_t \qquad (38)$$

with $\rho(\mathbf{x}, E_t, t)$ as the trapped hydrogen density $(\mathrm{cm}^{-3}\mathrm{eV}^{-1})$ at trap level E_t. Transport is governed by the continuity equation and the corresponding flux relation

$$\frac{\partial H}{\partial t} = -\nabla \cdot \mathcal{F} H_c + G_c. \qquad (39)$$

Note that in (39) the time derivative of the total hydrogen concentration is used which accounts for the exchange of particles with the trap levels. The occupancy of the trap levels is governed by balance equations which have to be solved for each trap level

$$\frac{\partial \rho(E_t)}{\partial t} = \underbrace{\frac{\nu}{N_c} \left(g(E_t) - \rho(E_t)\right) H_c}_{\text{capture}}$$
$$\underbrace{- \nu \exp\left(-\frac{E_c - E_t}{k_B T_L}\right) \rho(E_t)}_{\text{release}} \qquad (40)$$

with ν as the attempt frequency, N_c as the effective density-of-states in the hydrogen conduction band, and E_c as the hydrogen conduction band edge (assumed to be zero in the examples). An exponential density-of-states is commonly used [17], [25]

$$g(E_t) = \frac{N_t}{E_0} \exp\left(-\frac{E_c - E_t}{E_0}\right) \qquad (41)$$

which, in this particular context, results in a power law [17], [24] for the time dependence of ΔN_{it}. In the following, we restrict our discussion to a position-independent density-of-states. It is also worth recalling that the transport will only be dispersive for $E_0 > k_B T_L$, that is, for sufficiently "deep" trap distributions [25].

Qualitatively, the system responds as follows if brought out of equilibrium.

1) At the initial stage, the capture rate (first term) in (40) dominates. Since ρ will still be small, the distribution will closely resemble the density-of-states (cf., Fig. 5).
2) Then, since the release term depends exponentially on the distance in energy of the trap level from the conduction band, particles on shallower traps (traps "closer" to E_c) are more likely to be released than deeper traps. As a consequence, the shallower trap levels become depleted while particles accumulate in the "deep" traps. This is the nonequilibrium regime.
3) The transition between "shallow" and "deep" traps is described by the demarcation energy [24], [25], [51]

$$E_d(t) = E_c - k_B T_L \log(\nu t) \qquad (42)$$

which becomes more negative with time. Equation (42) is valid for $t > 1/\nu$.

4) As soon as the demarcation energy reaches the "bottom" of the density-of-states, equilibrium is obtained, and the system behaves similarly to a nondispersive one, although a different "effective" diffusivity and temperature dependence are observed [52]. Note, that from a mathematical point of view, this never happens for an ideal exponential density-of-states [25] such as (41).

The evolution of an initial particle sheet with time is shown in Fig. 4, whereas the trapped hydrogen profile $\rho(E_t, t)$ is shown in Fig. 5.

B. Arkhipov–Rudenko Approximation

As the MT equations are rather complex and can, in general, only be solved numerically, simplified equations have been derived by Arkhipov and Rudenko [25]. Their approximate solution relies on the existence of the demarcation energy separating shallow from deep traps and was derived to describe the broadening of an initial particle distribution in the hydrogen conduction band, such as in Fig. 4. This is not the case during NBT stress, however, where we have to deal with a continuous generation of particles at the interface during the stress phase. As the treatment of this generation term is fundamental for our considerations with respect to NBTI, an extended model is derived in the following.

Assuming a closed system with initial hydrogen concentration $H_0(\mathbf{x})$ in the conduction state and initially empty trap levels $(\rho(\mathbf{x}, E_t, t) = 0)$, we proceed by integrating the continuity (39) with respect to time to obtain

$$H(\mathbf{x}, t) - H_0(\mathbf{x}) = -\nabla \cdot \mathcal{F} \overline{H}_c(\mathbf{x}, t) + \overline{G}_c(\mathbf{x}, t). \qquad (43)$$

Here, we introduced the time average of a quantity as

$$\overline{X} = \int_0^t X(\mathbf{x}, t') dt'. \qquad (44)$$

The integral of the particle flux has been reformulated under the assumption that the flux operator $\mathcal{F}$ is time-independent. Most importantly, this requires $\mathbf{E}_{\text{ox}}$ to be independent of time. Assuming that the time-dependent demarcation energy (42) separates shallow from deep traps, that the trap occupancy can be neglected in the capture term of (40), that is, $g(E_t) \gg \rho(\mathbf{x}, E_t, t)$, and that the shallow traps ρ_s are in equilibrium with the conduction band $(\partial \rho_s(\mathbf{x}, E_t, t)/\partial t \approx 0)$, one can write from (40)

$$\rho_s(\mathbf{x}, E_t, t) = \frac{H_c(\mathbf{x}, t)}{N_c} g(E_t) \exp\left(\frac{E_c - E_t}{k_B T_L}\right). \qquad (45)$$

For the deep traps, the release term in (40) can be neglected, which results in

$$\rho_d(\mathbf{x}, E_t, t) = \frac{\nu}{N_c} \overline{H}_c(\mathbf{x}, t) g(E_t). \qquad (46)$$

Note that this assumes that the traps are initially empty, which is an assumption typical for current pulses in amorphous
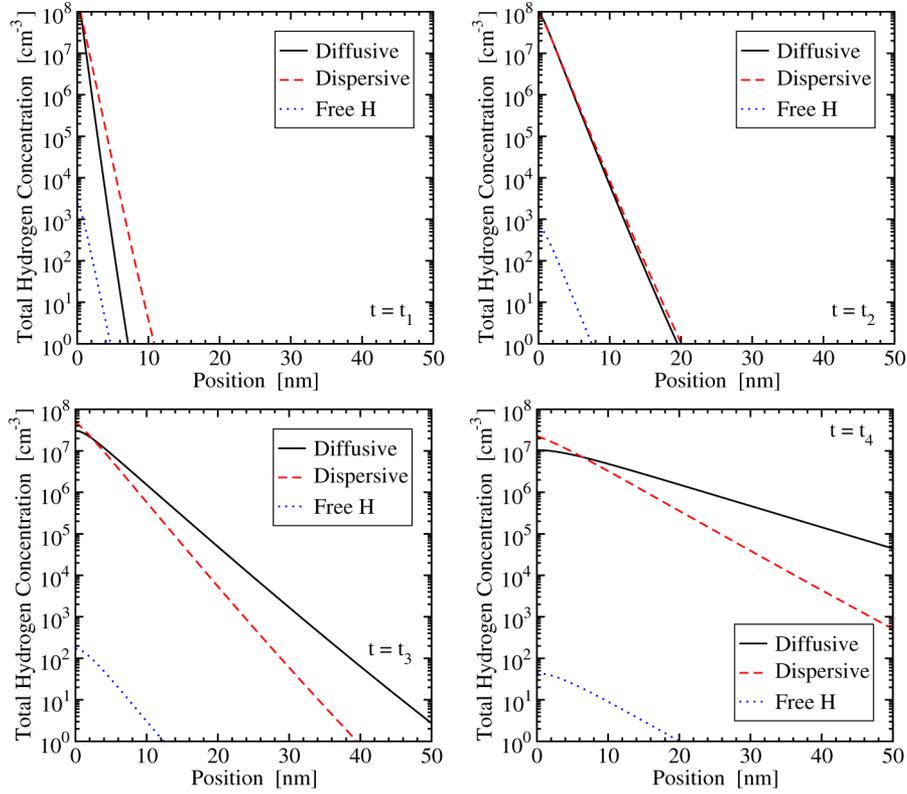
Fig. 4. Comparison of the hydrogen profiles at different time points for classic diffusion versus dispersive diffusion. Shown is the one-sided broadening of an initial particle sheet $H_0(x) = H_{\text{init}}\delta(x)$. For the classic case, the diffusivity was set to $D = D_c \times 10^{-4}$ in order to accommodate both profiles on the same plot. Note that the mobile hydrogen concentration in the conduction band H_c (dotted line) is much smaller than the concentration of the trapped hydrogen H_t (dashed line) and that the profile is steeper, that is, it remains closer to the initial position.

materials [47], but probably difficult to justify in the context of NBTI. The trapped hydrogen concentration can then be obtained as

$$H_t(\mathbf{x}, t) = \int_{E_d(t)}^{E_c} \rho_s(E_t)dE_t + \int_{-\infty}^{E_d(t)} \rho_d(E_t)dE_t \quad (47)$$

$$= \frac{H_c(\mathbf{x}, t)}{\theta(t)} + \frac{\overline{H}_c(\mathbf{x}, t)}{\tau(t)} \quad (48)$$

with the auxiliary functions

$$\frac{1}{\theta(t)} = \frac{1}{N_c} \int_{E_d(t)}^{E_c} g(E_t) \exp\left(\frac{E_c - E_t}{k_B T_L}\right) dE_t \quad (49)$$

$$\frac{1}{\tau(t)} = \frac{\nu}{N_c} \int_{-\infty}^{E_d(y)} g(E_t)dE_t. \quad (50)$$

For the sake of simplicity, we will restrict our discussion in the following to the exponential trap density-of-states (41) where the auxiliary functions can be explicitly given as

$$\tau(t) = \frac{1}{\nu} \frac{N_c}{N_t} (\nu t)^\alpha \quad (51)$$

$$\theta(t) \approx \tau(t)/(\alpha t) \quad (52)$$

with the dispersion parameter

$$\alpha = k_B T_L / E_0. \quad (53)$$

By adding H_c to the trapped hydrogen concentration (48), the total hydrogen concentration H can now be written as

$$H(\mathbf{x}, t) = H_c(\mathbf{x}, t) + H_t(\mathbf{x}, t) = \frac{H_c(\mathbf{x}, t)}{\gamma(t)\tau(t)} + \frac{\overline{H}_c(\mathbf{x}, t)}{\tau(t)} \quad (54)$$

with

$$\frac{1}{\gamma(t)} = \frac{1 + \theta(t)}{\theta(t)} \tau(t). \quad (55)$$

From (54), an explicit expression for $\overline{H}_c$ is obtained

$$\overline{H}_c(\mathbf{x}, t) = \tau(t)H(\mathbf{x}, t) - \frac{H_c(\mathbf{x}, t)}{\gamma(t)}. \quad (56)$$

Inserting (56) into (43) finally gives

$$H(\mathbf{x}, t) - H_0(\mathbf{x}) = -\nabla \cdot \mathbf{F}(\mathbf{x}, t) + \overline{G}_c(\mathbf{x}, t)$$
$$+ \frac{G_c(\mathbf{x}, t)}{\gamma(t)} - \frac{1}{\gamma(t)} \frac{\partial H(\mathbf{x}, t)}{\partial t}. \quad (57)$$

with

$$\mathbf{F}(\mathbf{x}, t) = \mathcal{F}\tau(t)H(\mathbf{x}, t). \quad (58)$$

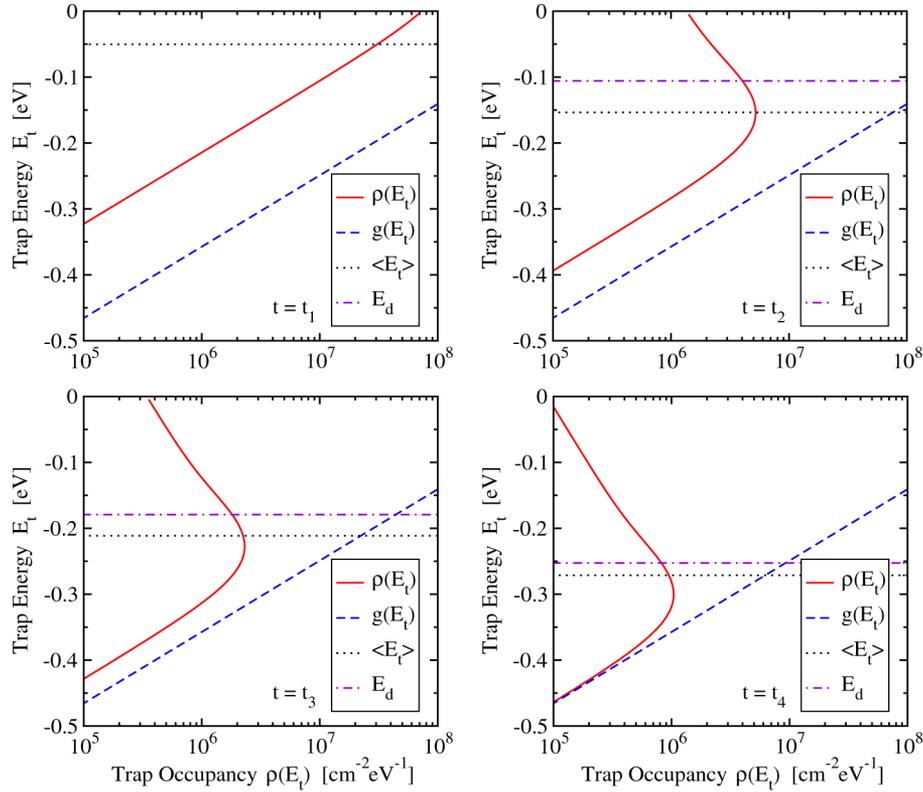By setting $G_0 = 0$, the original Arkhipov–Rudenko model is retained.

Fig. 5.   Evolution of the trapped hydrogen profile with time for the diffusion process given in Fig. 4. Shown is the density $\rho(E_t)$ right at the interface ($x = 0$). At early time points ($t = t_1$), the profile closely resembles the exponential density-of-states. Particles residing on shallow traps closer to $E_c = 0$ are easily emitted in a process that consequently favors the occupancy of the deeper trap levels. This results in the characteristic humps that can be observed for $t > t_1$. Note that the average energy of the trapped hydrogen $\langle E_t \rangle$ roughly corresponds to the demarcation energy E_d.

C. Extremely Nonequilibrium Arkhipov–Rudenko Approximation

For large times, (57) contains the transition to the equilibrium regime where most particles reside in shallow traps. Under the assumption that the system remains in nonequilibrium, (57) can be further simplified. In the nonequilibrium regime, most particles reside in the deep traps, which allows one to approximate the total hydrogen concentration as [25]

$$H(\mathbf{x}, t) = \frac{\overline{H_c}(\mathbf{x}, t)}{\tau(t)}. \tag{59}$$

Following the same procedure as before, one can derive an expression only valid in the extremely nonequilibrium case [25]

$$H(\mathbf{x}, t) - H_0(\mathbf{x}) = -\nabla \cdot \mathbf{F}(\mathbf{x}, t) + \overline{G_c}(\mathbf{x}, t) \tag{60}$$

to replace (57). Note that there is no time derivative in (60) because the dynamics of the system can be incorporated solely into $\tau(t)$, which directly depends on the hydrogen trap density-of-states and the demarcation energy. This is a characteristic feature of any adiabatic process, where the time dependence of the whole system is determined by the slowest process, in our case, the thermal equilibrium of hydrogen [53].

Of particular interest in our context is the concentration of the mobile hydrogen H_c, which is directly linked to the total

hydrogen concentration H through (59) as

$$H_c(\mathbf{x}, t) = \frac{\partial \tau(t) H(\mathbf{x}, t)}{\partial t}. \tag{61}$$

This relation will be used for the formulation of the NBTI boundary conditions.

D. Phenomenological Description of Dispersive Transport

Instead of MT or CTRW solutions, models based on a phenomenological time-dependent diffusivity

$$D(t) = D_{00}(\nu_0 t)^{\beta - 1} \tag{62}$$

have been used [2], [11], [20]. Here, D_{00} is the microscopic diffusivity, ν_0 is an attempt frequency [54] possibly different from ν, and β is the dispersion parameter [54]. As in the MT model for an exponentially decreasing trap density, β is given as $\beta = k_B T_L / E_\beta$, where E_β is the characteristic energy. Since (62) has been empirically formulated by matching for instance SIMS measurements, this model does not allow one to differentiate between mobile and trapped hydrogen, which has a significant influence on the NBTI boundary condition as shown later.

It is worth comparing the transport equation obtained with the time-dependent diffusivity to the approximate solution of the MT equations. Inserting (62) into (4) gives

$$\frac{\partial H}{\partial t} = -\nabla \cdot \frac{D(t)}{D_c} \mathcal{F} H + G_c. \tag{63}$$

Conversely, by taking the time-derivative of the nonequilibrium MT approximation (60), one obtains

$$\frac{\partial H}{\partial t} = -\nabla \cdot \frac{\partial \tau}{\partial t} \mathcal{F} H - \nabla \cdot \tau \mathcal{F} \frac{\partial H}{\partial t} + G_c. \tag{64}$$

The most notable difference to the phenomenological description (63) is a different treatment of the particle flux, which, in (64), has already been reformulated in order to allow a comparison. For an exponential trap density-of-states, a comparison of the prefactor of the first flux term in (64) with the coefficient appearing in (63) yields that both fluxes are equivalent provided that

$$D_c \alpha \frac{N_c}{N_t} (\nu t)^{\alpha-1} = D_{00} (\nu_0 t)^{\beta-1} \tag{65}$$

holds. This is obviously the case if, for instance, $\alpha = \beta$, $\nu = \nu_0$, and $D_{00} = D_c \alpha N_c / N_t$. Thus, for the special case that $\partial H / \partial t$ is small, the phenomenological formulation is equivalent to the nonequilibrium MT approximation. This result will be used in the discussion of the Zafar model (cf., Section VI-B). Interestingly, for proton transport, the condition $\partial H / \partial t \approx 0$ is approximately valid during the initial drift-limited phase, which allows one to neglect the second flux term in (64).

IV. DISPERSIVE TRANSPORT AND NBTI

In order to obtain an NBTI model, the dispersive transport equation has to be coupled to the electro-chemical reaction assumed to take place at the interface. For the present analysis, we have to keep in mind that the macroscopic density-of-states is derived for an amorphous bulk material and is unlikely to be valid close to an interface. In that context, the physical mechanisms justifying the "conduction band" concept in conjunction with hydrogen hopping next to the interface need to be evaluated and justified. Published dispersive NBTI models, however, are based on the validity of this concept, and the different interpretations explain the discrepancies in these models.

As in the RD model, the kinetic equation describing the interface reaction is assumed to be of the form (3). Also, the interface reaction is assumed to be in quasi-equilibrium, that is, (9) to hold. In the following, various analytical models will be derived using different boundary and initial conditions based on the extremely nonequilibrium transport (60).

The time average of the generation term required in (60) follows directly from (6) as

$$\overline{G}_c(\mathbf{x}, t) = \frac{\Delta N_{\text{it}}(t)}{a} \delta(x - x_0). \tag{66}$$

By placing the interface at $x = 0$, the total hydrogen concentration in the positive half-space can be given at every time step through

$$H(x, t) = H(0, t) \exp\left(-\frac{x}{\lambda(t)}\right) \tag{67}$$

with $\lambda(t) = \sqrt{D_c \tau(t)}$ for neutral particles and $\lambda(t) = \mu_c E_{\text{ox}} \tau(t)$ for protons [17]. For the exponential trap density-of-states, one obtains for neutral particles

$$\lambda(t) = \left(\frac{D_c}{\nu} \frac{N_c}{N_t}\right)^{1/2} (\nu t)^{\alpha/2} \tag{68}$$

whereas the proton results in

$$\lambda(t) = \frac{D_c}{\nu} \frac{N_c}{N_t} \frac{E_{\text{ox}}}{V_T} (\nu t)^{\alpha}. \tag{69}$$

Note that (69) is only valid for larger times as it neglects the diffusive component at short times [17] and, as in the RD model, H^+ will at first behave like H^0.

Using the spatial distribution of the total hydrogen concentration (67), the continuity equation for the extremely nonequilibrium case (60) can be integrated over the half-space $x > 0$, and one obtains with the assumption $H_0(\mathbf{x}) = 0$

$$H(0, t) = \frac{\Delta N_{\text{it}}(t)}{a \lambda(t)}. \tag{70}$$

By identifying $B(t) = \lambda(t)$, (70) is the dispersive equivalent of (12) obtained for the standard RD model. A compilation of the values of B for the three discussed species is given in Table I.

Alternatively, we can integrate the MT continuity (60) over an infinitesimally thin interfacial layer to obtain

$$\mathbf{F}(0, t) \cdot \mathbf{n} = \frac{\Delta N_{\text{it}}(t)}{a}. \tag{71}$$

It is straightforward to show that $\mathbf{F} \cdot \mathbf{n} = \lambda H$ holds for the exponential hydrogen profile (67). Thus, for the dispersive MT model, we only need to consider the single fundamental equation (9). This is of course a consequence of the fact that we can use the exact solution for the hydrogen profile rather than an approximation as in the RD case.

A crucial question in the context of dispersive transport is how to determine the interfacial hydrogen concentration H_{it}. In the following, we will consider two different models. The first assumes that H_{it} is given by the total hydrogen concentration H, thus, from (9) and (70)

$$\left(\frac{k_f}{k_r} \frac{\Delta N_{\text{it,max}} - \Delta N_{\text{it}}}{N_{\text{it0}} + \Delta N_{\text{it}}}\right)^a = \frac{\Delta N_{\text{it}}}{aB}. \tag{72}$$

This is the assumption employed in the Kaczer–Arkhipov model [17]. The different behavior observed in the dispersive case is therefore the consequence of a modified $B(t)$.

Alternatively, one may assume that only the mobile hydrogen can contribute to the reverse reaction, that is, $H_{\text{it}} = H_c$, and we obtain via (9), (61), and (70)

$$\left(\frac{k_f}{k_r} \frac{\Delta N_{\text{it,max}} - \Delta N_{\text{it}}}{N_{\text{it0}} + \Delta N_{\text{it}}}\right)^a = \frac{\partial}{\partial t} \frac{\tau \Delta N_{\text{it}}}{aB}. \tag{73}$$

Here, the different behavior is a consequence of a modified B, τ, and time derivative. As will be shown, this results in a fundamentally different behavior compared to the Kaczer–Arkhipov model. In the following, the four solutions of (72) and (73) for the cases $\Delta N_{\text{it}}(t) \gg N_{\text{it0}}$ and $\Delta N_{\text{it}}(t) \ll N_{\text{it0}}$ are analyzed.

A. Total Hydrogen Boundary Condition, RDD Regime

The solution of (72) can be directly taken from the generalized RD model discussed in the previous sections using $B = \lambda$. Thus, in the RDD regime, we obtain from (23) for neutral particles

$$\Delta N_{\text{it}}(t) = A_{\text{RD}} \left(\frac{D_c}{\nu} \frac{N_c}{N_t} \right)^{1/(2+2a)} (\nu t)^{\alpha/(2+2a)} \qquad (74)$$

with the same prefactor A_{RD} as in the RD model given through (24). For atomic hydrogen ($a = 1$), the exponent is given through $n = \alpha/4$, whereas molecular hydrogen ($a = 2$) gives $n = \alpha/6$.

For the proton, we obtain from the approximate relation for $\lambda(t)$

$$\Delta N_{\text{it}}(t) = A_{\text{RD}} \left(\frac{D_c}{\nu} \frac{N_c}{N_t} \frac{E_{\text{ox}}}{V_T} \right)^{1/2} (\nu t)^{\alpha/2}. \qquad (75)$$

Note that the numerical solution for H^+ may contain a transitional regime with $n = \alpha/4$, where the diffusive component still dominates.

Since α is equal to one in the diffusive limit and zero in the extremely dispersive case, (74) and (75) imply that, with dispersive transport, an exponent smaller than the RD exponents of 1/2, 1/4, and 1/6 can be obtained. Also, for increasing trap density N_t, the total amount of degradation decreases.

A qualitative explanation of the exponent reduction can be given by noting that dispersive transport results in most particles being trapped close to the interface, yielding a steeper profile compared to classic diffusion. As all hydrogen is available for the reverse rate in (3), the net interface state generation is suppressed, resulting in a smaller exponent.

Since the dispersion parameter α depends linearly on the temperature, a linear temperature dependence of the exponent is obtained as [17]

$$n_1 = \frac{\alpha}{2 + 2a} = \frac{k_B T_L}{2 E_0 (1 + a)}. \qquad (76)$$

This is consistent with experimental results obtained with delayed measurements [3], [17], but inconsistent with the delay-free measurement results of [9], [29].

B. Total Hydrogen Boundary Condition, Pre-RDD Regime

For the case that a large initial concentration of interface states is allowed, the pre-RD result (26) can be directly applied,
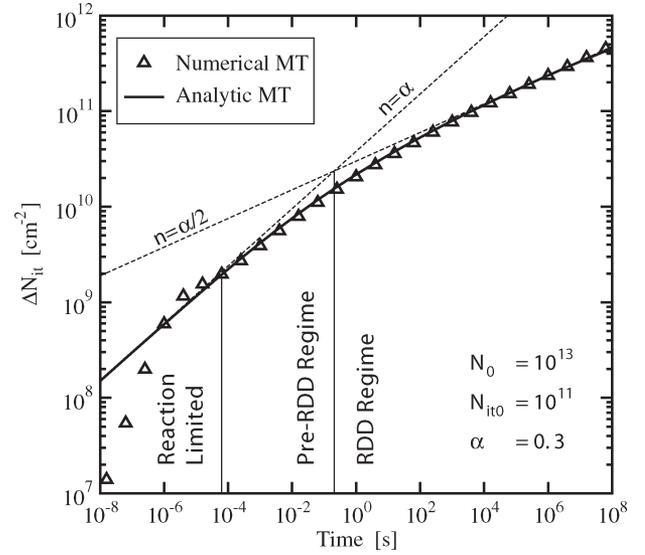

Fig. 6. Example simulation showing the transition between the pre-RDD regime and the RDD regime which could be used to explain a different initial exponent compared to the long time exponent. Shown are the numerical and analytical solutions of the MT equations. Note that the analytical solution is only valid after the reaction-limited phase.

and one obtains with the dispersive area function for neutral species (68)

$$\Delta N_{\text{it}}(t) = A_P \left(\frac{D_c}{\nu} \frac{N_c}{N_t} \right)^{1/2} (\nu t)^{\alpha/2}. \qquad (77)$$

For the proton, one obtains with (69)

$$\Delta N_{\text{it}}(t) = A_P \frac{D_c}{\nu} \frac{N_c}{N_t} \frac{E_{\text{ox}}}{V_T} (\nu t)^{\alpha}. \qquad (78)$$

As before, the exponents $n = \alpha$, $\alpha/2$, and $\alpha/2$ for H^+, H^0, and H_2 reduce to their pre-RD equivalents 1, 1/2, and 1/2 for $\alpha = 1$. Also, the exponent increases linearly with temperature similarly to (76), and the same compatibility/incompatibility to measurements is given.

Interestingly, (78) shows the same characteristic features as the Zafar model, that is, $n = \alpha$ and $\Delta N_{\text{it}} \propto D_c$. This similarity is further discussed in Section VI-B.

Another interesting interpretation following from a transition between the pre-RDD to the RDD regime is as follows. It has been reported [9], [41], [42] that the initial power-law exponent observed during measurements is close to 0.3, which later-on changes to a value close to 0.15. This has been attributed to H^0–H_2 conversion. In the dispersive transport framework, however, a different interpretation becomes possible: For H^+ and H^0 transport, the ratio of the exponents in the pre-RDD and RDD regimes is two, so with a dispersion parameter of $\alpha = 0.3(H^+)$ or $\alpha = 0.6(H^0)$ a transition from 0.3 to 0.15 would be predicted. The full solution of this transition for $a = 1$ can be directly transferred from the generalized RD result (30) and $B = \lambda$. A possible transition between the pre-RDD and the RDD regime is shown in Fig. 6.

C. Conduction State Hydrogen BC, RDD Regime

The previous two models were based on the assumption that all hydrogen (mobile and trapped) can participate in the NBTI reverse rate. In contrast, if we now assume that only the mobile hydrogen can participate in the reverse rate, that is, $H_{it} = H_c(0)$, which appears to be the "natural" boundary condition for the MT model [55], one obtains [see Appendix, (93)]

$$\Delta N_{it}(t) = \frac{a\lambda(t)}{\tau(t)}$$
$$\times \left((1+a)\left(\frac{k_f}{k_r}N_0\right)^a \int_{t_0}^{t} \left(\frac{\tau(t')}{a\lambda(t')}\right)^a dt' \right)^{1/1+a} \quad (79)$$

For neutral particles, (79) results in

$$\Delta N_{it}(t) = A_{RD} \left(\frac{D_c}{\nu}\frac{N_t}{N_c}\right)^{1/(2+2a)} \left(\frac{1+a}{1+a\alpha/2}\right)^{1/(1+a)}$$
$$\times (\nu t)^{(1-\alpha/2)/(1+a)}. \quad (80)$$

For atomic hydrogen, the exponent $n = 1/2 - \alpha/4$ is obtained, whereas H_2 results in $n = 1/3 - \alpha/6$. Hence, for increased dispersion, the exponents now become larger than their RD equivalents. Furthermore, when the trap density is increased, the degradation increases. This is in agreement with the previously stated result that the inclusion of traps into a standard RD model increases the exponent [7], [12].

Interestingly, for H^+, the time dependence of $\lambda(t)$ cancels with $\tau(t)$, thereby reducing (93) to

$$\Delta N_{it}(t) = \left(2\frac{k_f N_0}{k_r}D_c\frac{E_{ox}}{V_T}\right)^{1/2} t^{1/2} \quad (81)$$

with an exponent $n = 1/2$, incompatible with measurements. This is equal to the classic result (25) obtained from the more exact flux formulation and independent of the dispersion parameter.

Again, qualitatively, in this model, the newly released hydrogen quickly falls into the traps, but for times larger than $1/\nu$, most hydrogen resides in deep traps and is therefore not as easily available for the reverse rate in (3). This suppresses the reverse reaction and consequently enhances the net interface state generation and results in a larger exponent.

In contrast to the total hydrogen boundary condition, now the exponent decreases with increasing temperature through

$$n_2 = \frac{1-\alpha/2}{1+a} = \frac{2E_0 - k_B T_L}{2E_0(1+a)} = \frac{1}{1+a} - n_1. \quad (82)$$

This is in contradiction to currently available observations [3], [9], [17]. Note, however, that this particular temperature dependence is a consequence of the exponential trap density-of-states, and a hardly noticeable temperature dependence has been reported [12] using a Gaussian distribution on top of the exponential density-of-states.

D. Conduction State Hydrogen BC, Pre-RDD Regime

The last case that we consider is the pre-RDD regime obtained under the assumption that only hydrogen in the conduction state can contribute to the reverse reaction. As shown in the Appendix [see (95)], for $\Delta N_{it}(t) \ll N_{it0}$, we obtain

$$\Delta N_{it} = A_P \frac{\lambda(t)}{\tau(t)} t. \quad (83)$$

For neutral species, this gives

$$\Delta N_{it} = A_P \left(\frac{D_c}{\nu}\frac{N_t}{N_c}\right)^{1/2} (\nu t)^{1-\alpha/2}. \quad (84)$$

As in the RD case, the exponent is independent of the kinetic exponent a and is solely given by the shape function λ. For the proton, one obtains

$$\Delta N_{it}(t) = A_P D_c \frac{E_{ox}}{V_T} t. \quad (85)$$

Again, the exponent is independent of the dispersion parameter and is equal to one. As such, this regime would be similar to the reaction-limited phase of the standard RD model. Also, the temperature dependence of the exponent is in contradiction to the measurement data, as are the very large exponent values, making the applicability of this particular model rather unlikely.

V. COMPARISON AND DISCUSSION

In the following, the analytical NBTI models using the possible combinations of boundary and initial conditions given in the previous section will be compared to their corresponding numerical solution. For the numerical solution, the trap density-of-states was discretized using 20 energy points, whereas the energy range was limited to the interval $E_{max} = 0$ eV and $E_{min} = -20 E_0$. This implies that, as soon as the demarcation energy E_d reaches E_{min}, a transition from the nonequilibrium dispersive to the equilibrium diffusive regime is observed. Note that this transition is, of course, not available in the approximate solutions described earlier. As the exact value of E_{min} is essentially unknown, it was set to a value small enough so as not to influence the numerical solution. Furthermore, the numerical solution considers the trap occupancy in the capture rate of (40), which is also not contained in the approximate solutions. In addition, this trap occupancy results in a transition from dispersive to conventional diffusion as soon as all traps are filled. Such a transition might be relevant and can also be experimentally observed in hydrogen diffusion experiments for hydrogen concentrations larger than the trap density [20]. However, this effect is neglected here for the sake of a straightforward comparison.

In the first step, the applicability of the Arkhipov–Rudenko model to NBTI is investigated. For this, the numerical solutions of the MT equations and the extremely nonequilibrium approximation (EN-MT) are compared in Fig. 7, where good agreement is observed for each boundary condition, thereby justifying the underlying approximations. Next, the analytical
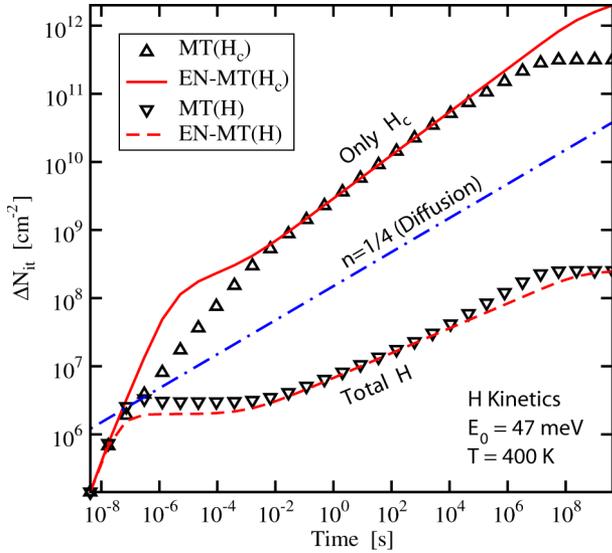
Fig. 7. Interface state density as a function of the boundary condition calculated numerically by solving the MT and extremely nonequilibrium MT (EN-MT) equations with $N_{it0} = 0$. Saturation occurs as soon as the hydrogen diffusion front reaches the other side of the oxide layer, where a perfectly reflecting boundary condition was used in the numerical solutions. The approximations underlying the EN-MT equations seem to be well justified.
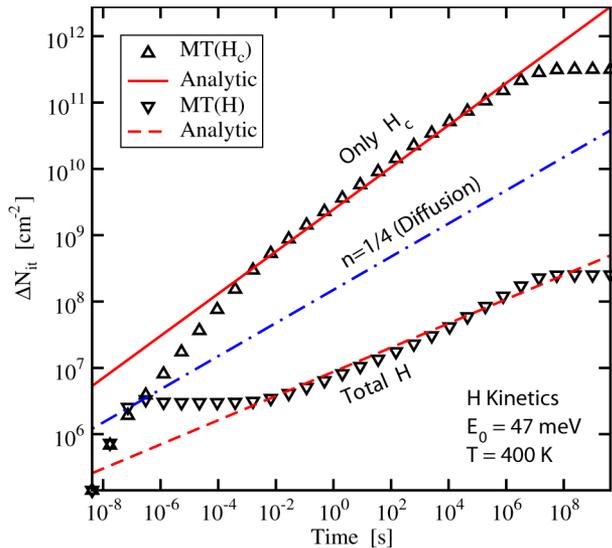

Fig. 8. Interface state density as a function of the boundary condition calculated numerically by solving the MT equations in comparison to the analytical expressions (74) and (80) for $N_{it0} = 0$. Again, good agreement is obtained for both boundary conditions.

expressions (74) and (80) are compared to the numerical solutions of the MT equations in Fig. 8. Again, good agreement is obtained in the quasi-equilibrium (diffusion-limited) regime. Of course, no reaction-limited regime and saturation can be observed in these analytical models.

The temperature dependence of the exponents predicted by the analytical expressions (74) and (80) is compared to the full numerical results in Fig. 9. Note that the system is only dispersive as long as the characteristic energy E_0 in the density-of-states (41) is larger than the thermal energy $k_B T_L$ [25]. In terms of the dispersion parameter α, this means $\alpha < 1$. This
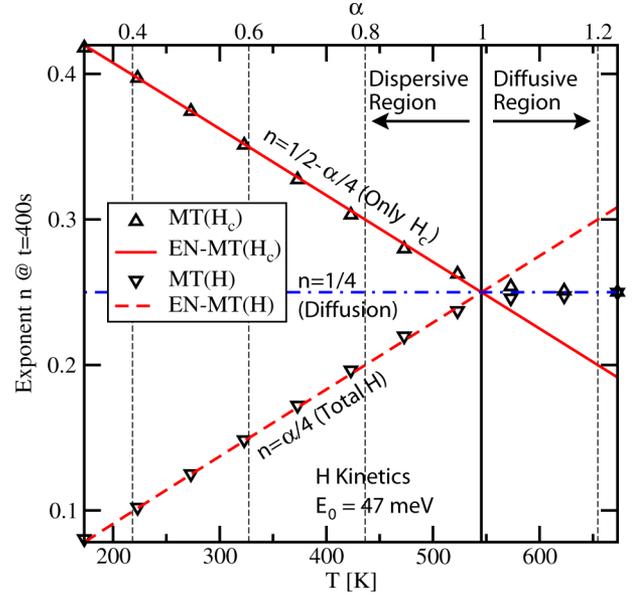

Fig. 9. Temperature dependence of the exponent for the two boundary conditions. As expected from the derivation, the EN-MT model breaks down for the case when the trap density-of-states becomes too narrow for dispersive transport to occur ($\alpha > 1$), whereas the MT model correctly reproduces the diffusive limit with $n = 1/4$.

also implies that, for increasing temperature, a transition to classic transport is observed as soon as E_0 becomes smaller than the thermal energy $k_B T_L$, that is, $\alpha > 1$. Since the dispersive models are derived under the assumption $\alpha < 1$, they can, of course, not reproduce the full numerical results in that regime, but give excellent agreement for $\alpha < 1$.

The good agreement between the numerical and analytical result indicates that the simplifying assumptions in the derivation of (74) and (80) are well justified, which are worth summarizing.

1) The dynamics are solely determined by carrier trapping and detrapping.
2) The continuous injection of particles is too slow ($\partial N_{it}/\partial t \approx 0$) to seriously disrupt the extremely nonequilibrium assumption with a single demarcation energy.
3) The amount of hydrogen that is allowed to participate in the NBTI reverse reaction determines the overall dynamics, that is, this boundary condition determines whether an increase or a decrease in the exponent is observed.
4) The interface reaction is in quasi-equilibrium.

The possible exponents for the various combinations of boundary condition and species are compared in Fig. 10. The fractional power-law exponents obtained from the various combinations of boundary and initial conditions are summarized in Table II. The darker the box around a particular combination, the less likely the model is to be correct. This assessment is based on the ability of the model to reproduce results of measurements with delay. We repeat that these models cannot reproduce a temperature-independent power-law exponent in delay-free measurements.
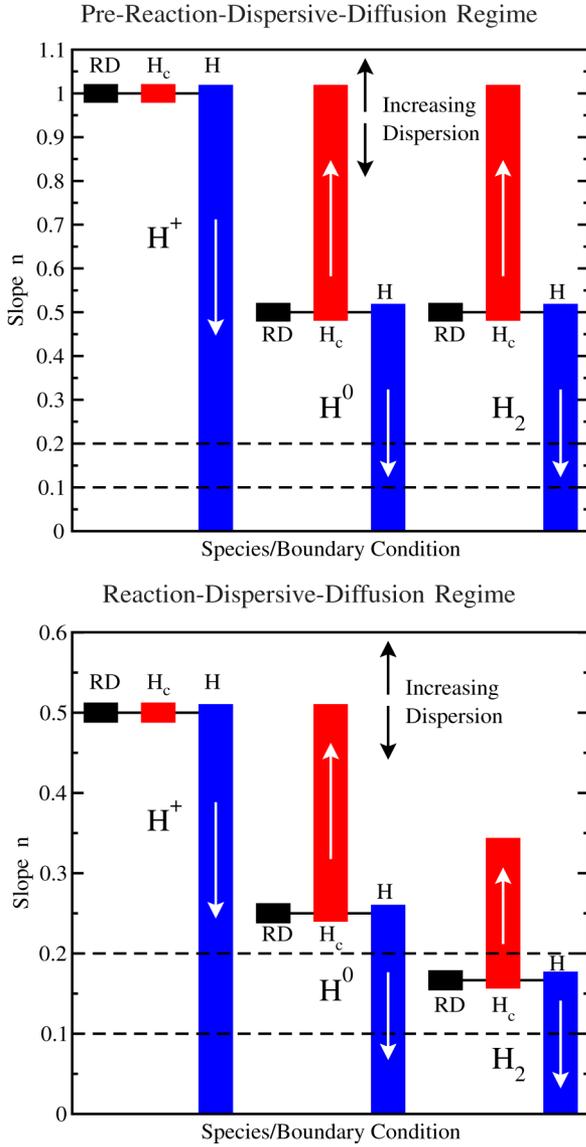
Pre-Reaction-Dispersive-Diffusion Regime

Reaction-Dispersive-Diffusion Regime

Fig. 10. Possible exponents for the two boundary conditions and the three investigated species (H^+, H^0, and H_2). The top figure shows the result for the pre-RD regime, whereas the bottom figure gives the traditional RD regime. For the boundary condition $H_{it} = H_c$, an exponent larger than the RD equivalent is obtained, whereas the boundary condition $H_{it} = H$ results in the opposite behavior. Also, (roughly) indicated is the range of exponents observed during on-the-fly measurements $n \approx 0.1-0.2$.

TABLE II
POSSIBLE POWER-LAW EXPONENTS

	H^+	H^0	H_2
Pre-RD	$1/2\ldots1$	$1/2$	$1/2$
RD	$1/4\ldots1/2$	$1/4$	$1/6$
Pre-RDD, $H_{it} = H_t$	$\alpha/2\ldots\alpha$	$\alpha/2$	$\alpha/2$
RDD, $H_{it} = H_t$	$\alpha/4\ldots\alpha/2$	$\alpha/4$	$\alpha/6$
Pre-RDD, $H_{it} = H_c$	$1-\alpha/2\ldots1$	$1-\alpha/2$	$1-\alpha/2$
RDD, $H_{it} = H_c$	$1/2-\alpha/4\ldots1/2$	$1/2-\alpha/4$	$1/3-\alpha/6$

VI. ALTERNATIVE MODELS

In addition to the MT-based models discussed so far, formulations using alternative dispersive hydrogen transport models
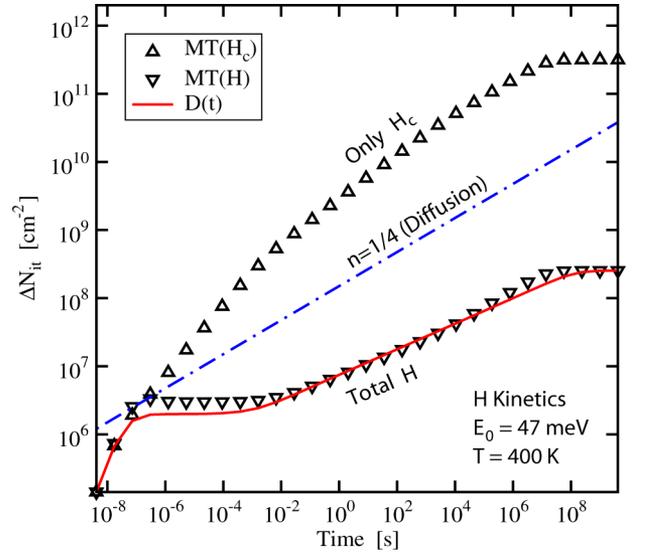

Fig. 11. Comparison of the calculated interface state density obtained by numerically solving the diffusion equation with a time-dependent diffusivity for $N_{it0} = 0$. Good agreement for the case $H_{it} = H$ is obtained.

have been developed. These are summarized in the following and compared to the previously derived models.

A. Phenomenological Dispersive RD Model

Based on the phenomenological diffusivity (62), Alam and Mahapatra first discussed dispersive hydrogen transport in connection with the RD model [2]. By inserting (62) into (15), one obtains for the area estimator

$$B(t) = \lambda_0 \left(\frac{D_{00}}{\nu_0}\right)^{1/2} (\nu_0 t)^{\beta/2} \tag{86}$$

which is essentially the same as (68), except for a time-independent prefactor. For the proton, one obtains with (17)

$$B(t) = \frac{D_{00}}{\nu_0} \frac{E_{ox}}{V_T} (\nu_0 t)^{\beta} \tag{87}$$

which is also essentially the same as (69). Consequently, as the power-law exponents are determined through the hydrogen profile shape functions λ, the same time dependence as in the simplified MT models based on the total hydrogen boundary condition is obtained from that treatment, both for the pre-RDD and the RDD regime. The values of B for the three species are compared to the other theories in Table I.

The numerical solution of a standard RD model with such a time-dependent diffusivity is shown in Fig. 11. As also demonstrated in the analytical analysis, the simple phenomenological model captures the case where the total hydrogen participates in the reverse rate ($H_{it} = H$) very well.

B. Statistical Mechanics Proton Transport Model

As in the discussion on dispersive transport by Alam and Mahapatra, the model proposed by Zafar [11] also uses the phenomenological description of the diffusivity (62). The electrochemical reaction at the interface is replaced by invoking

assumptions based on statistical mechanics, which for protons results in

$$N_i \exp\left(-\frac{E_i}{k_B T_L}\right) \frac{N_0 - N_{\mathrm{it}}}{N_{\mathrm{it}}} = H_{\mathrm{it}}. \qquad (88)$$

Here, N_i is the total density of interstitial sites at the interface, and E_i is the energy required to create interstitial hydrogen at the interface. Comparison with the standard RD interface reaction in quasi-equilibrium (9) shows that (88) is equivalent provided that

$$\frac{k_f}{k_r} = N_i \exp\left(-\frac{E_i}{k_B T_L}\right). \qquad (89)$$

As in the RD model, the rates k_f and k_r are assumed to follow an Arrhenius activation law [2]. The interface reaction (88) is equivalent from a mathematical point of view, although the interpretation of the parameters is somewhat different (see [11] for additional details).

Since the Zafar model uses the flux-based formalism, it results in a stretched-exponential, provided that $\Delta N_{\mathrm{it}} \ll N_0$ holds. With $C_0 = D_{00}\nu^{\beta-1}E_{\mathrm{ox}}/V_T$ and $c = \beta$, the results obtained in Section II-D can be directly transferred, and the saturation behavior is given by (36).

In Fig. 12, the numerical solution of the MT model is compared to a numerical solution of the implicit solution (33), the stretched-exponential approximation (36), which is the power-law-like approximation of the MT model (31) for two different initial values of interface states N_{it0}. This comparison confirms the previously drawn conclusions.

1) The analytical expressions derived from the flux formulation give very accurate results. Only in the saturation regime, the analytical approximations produce slightly larger values, whereas the numerical solution gives a somewhat smoother transition.
2) The stretched-exponential (36) is a good approximation, provided that $N_{\mathrm{it0}} \approx N_0$. In that case, the power-law-like expression (31) and the stretched-exponential give very similar results.
3) For $N_{\mathrm{it0}} = N_0/10$, however, the condition $N_{\mathrm{it0}} \ll N_0$ is not fulfilled, resulting in a large error of the stretched-exponential approximation. The power-law-like expression is always correct for small times, whereas it gives a slight overestimation during saturation.

C. CTRW Model

Instead of the MT model, an approximate solution for the CTRW model was employed by Houssa *et al.* [16]. Approximate CTRW solutions are commonly derived using simplified trial functions [21], [22]. Again, the approximate solution used for NBTI [16] was originally devised for the broadening of an initial sheet of particles created during a radiation pulse. Since CTRW and MT theory are in many ways compatible [48], [49], we assume our results of the MT model to also apply to models derived from the CTRW theory. The derivation given by Houssa *et al.* [16] uses dispersive proton transport, the total hydrogen concentration for the backward rate, and a small
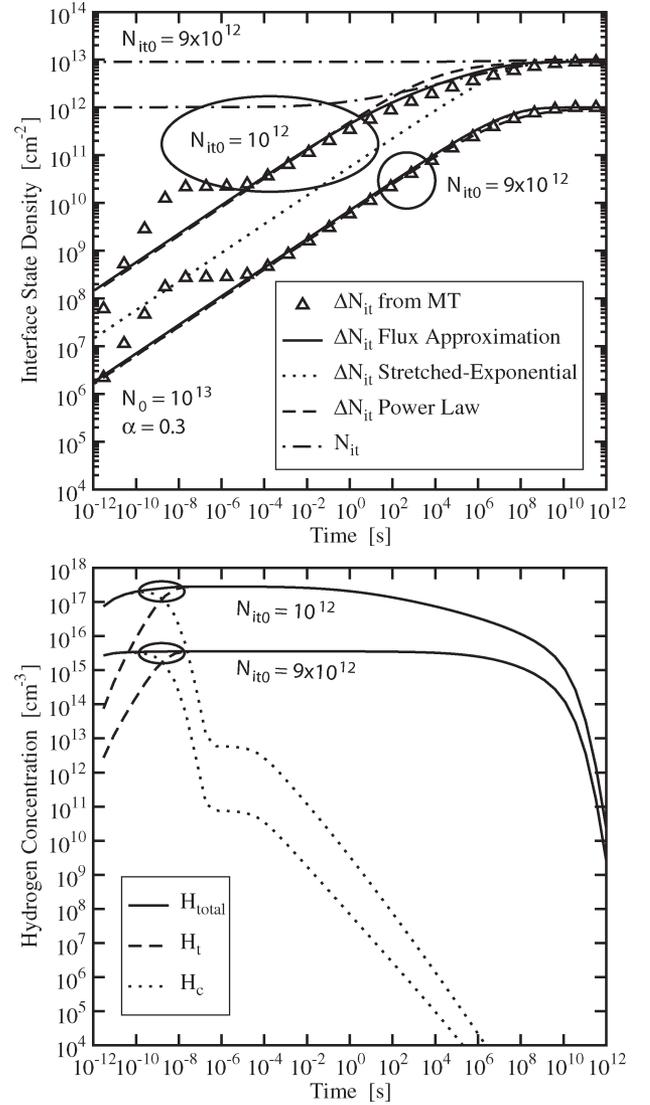

Fig. 12. (Top) The evolution of ΔN_{it} with time as obtained from the MT model with the total hydrogen BC and a large initial density of interface states ($N_{\mathrm{it0}} = 9 \times 10^{12}$ cm^{-2}, $N_0 = 10^{13}$ cm^{-2}) in comparison to the analytical expressions given by the power-law-like expression (31) and the stretched-exponential given by Zafar (36). A very good agreement is obtained for $t > 0.1$ ms (beginning of the diffusion limited phase) and during the saturation phase. For smaller values of the initial density of interface states, however, $N_{\mathrm{it0}} = 10^{12}$ cm^{-2}, the stretched-exponential becomes rather inaccurate. Note that the saturation in both models is due to hard saturation. (Bottom) The evolution of the interfacial hydrogen concentration (total, trapped, and mobile), which shows that the total hydrogen concentration is roughly constant during the stress phase.

initial concentration of interface states. As such, the results should be comparable to the Kaczer–Arkhipov model (75). Indeed, the exponents given in [16, Fig. 2] roughly follow $\alpha/2$, although there appears to be a nonlinearity for intermediate values of α. This could, for instance, be the result of a simplified trial function or a numerical artifact.

VII. CONCLUSION

Recently, a large number of NBTI models have been proposed, which owe many of their properties to the drift or

diffusion of a hydrogen species released from previously passivated dangling bonds. Although relying on seemingly similar physical assumptions, these models result in rather different predictions for the creation of interface defects. In order to understand these differences, we employed a generalized RDD framework to study the influence of the boundary and initial conditions on the final NBTI model. It has been shown that the solutions obtained from the approximate transport models agree very well with the more rigorous results based on the dispersive MT transport model. A clear link between the various published RDD models could be established, which has been shown to originate from a different treatment of these boundary and initial conditions. Clearly, the question of what boundary condition for the reverse rate in the NBTI model captures the microscopic physics best is of utmost importance. In addition, the optimum interpretation of the hard saturation value of the interface states needs to be clarified.

Under the assumption that the concept of a bulk trap density-of-states remains valid next to the interface, we have investigated two different boundary conditions: Provided that only hydrogen in the MT conduction band can passivate dangling bonds, only H_2 in an RDD model gives exponents within the measurement range and would allow to explain delay-free exponents larger than 1/6. However, these exponents would depend on temperature, which has, so far, only been observed in delayed measurements. The influence of the trap density-of-states on temperature dependence needs to be investigated in that context, and an exponential density-of-states gives results in contradiction with measurements. In contrast, if all the trapped hydrogen can be involved, the previously published NBTI models [2], [11], [16], [17] are accurate, reproducing (temperature dependent) measured exponents also with H^0 and H^+ kinetics. Based on the ideas of Zafar, a pre-RDD regime has been introduced, which shows the same qualitative dependence on the boundary condition and results in a decreasing exponent with increasing dispersion for the total hydrogen boundary condition. It has been shown that, depending on the initial value of the interface state density, the pre-RDD, the RDD, or a transition between both regimes is observed. Finally, it has been shown that the Zafar model can be considered a special case of the presented generalized RDD model.

APPENDIX

In the following, the solution for the generalized RDD equation in the diffusion-limited regime is derived using only the conduction state hydrogen for the reverse rate boundary condition. We start with

$$\left(\frac{k_f}{k_r} \frac{N_0 - N_{it0} - \Delta N_{it}}{N_{it0} + \Delta N_{it}} \right)^a = \frac{\partial U \Delta N_{it}}{\partial t} \quad (90)$$

with the auxiliary function $U(t) = \tau/(a\lambda)$, which will be solved for the two limiting cases $\Delta N_{it} \gg N_{it0}$ and $\Delta N_{it} \ll N_{it0}$ in the following. Saturation effects will be neglected, that is, $\Delta N_{it} \ll N_0$, in order to obtain meaningful simple analytical expressions.

A. Small Initial Concentration of Interface States

For $\Delta N_{it} \gg N_{it0}$ and $\Delta N_{it} \ll N_0$, (90) can be simplified to

$$\left(\frac{k_f}{k_r} \frac{N_0}{\Delta N_{it}} \right)^a = \frac{\partial U \Delta N_{it}}{\partial t}. \quad (91)$$

After some algebraic manipulations, this can be rewritten as a first-order ordinary differential equation

$$\frac{U}{1+a} \frac{\partial \Delta N_{it}^{1+a}}{\partial t} + U' \Delta N_{it}^{1+a} = \left(\frac{k_f}{k_r} N_0 \right)^a. \quad (92)$$

The aforementioned expression can be solved in a standard manner to obtain

$$\Delta N_{it} = \frac{1}{U} \left((1+a) \left(\frac{N_0 k_f}{k_r} \right)^a \int_{t_0}^{t} U(t')^a dt' \right)^{1/(1+a)}. \quad (93)$$

B. Large Initial Concentration of Interface States

For $\Delta N_{it} \ll N_{it0}$, (90) can be simplified to

$$\left(\frac{k_f}{k_r} \frac{N_0 - N_{it0}}{N_{it0}} \right)^a = \frac{\partial U \Delta N_{it}}{\partial t} \quad (94)$$

and solved in a straightforward manner to give

$$\Delta N_{it} = \left(\frac{k_f}{k_r} \frac{N_0 - N_{it0}}{N_{it0}} \right)^a \frac{t}{U}. \quad (95)$$

ACKNOWLEDGMENT

REFERENCES

[1] D. K. Schroder and J. A. Babcock, "Negative bias temperature instability: Road to cross in deep submicron silicon semiconductor manufacturing," *J. Appl. Phys.*, vol. 94, no. 1, pp. 1–18, Jul. 2003.

[2] M. A. Alam and S. Mahapatra, "A comprehensive model of PMOS NBTI degradation," *Microelectron. Reliab.*, vol. 45, no. 1, pp. 71–81, Jan. 2005.

[3] V. Huard, M. Denais, and C. Parthasarathy, "NBTI degradation: From physical mechanisms to modelling," *Microelectron. Reliab.*, vol. 46, no. 1, pp. 1–23, Jan. 2006.

[4] J. H. Stathis and S. Zafar, "The negative bias temperature instability in MOS devices: A review," *Microelectron. Reliab.*, vol. 46, no. 2–4, pp. 270–286, Feb.–Apr. 2006.

[5] K. O. Jeppson and C. M. Svensson, "Negative bias stress of MOS devices at high electric fields and degradation of MNOS devices," *J. Appl. Phys.*, vol. 48, no. 5, pp. 2004–2014, May 1977.

[6] S. Ogawa and N. Shiono, "Generalized diffusion–reaction model for the low-field charge-buildup instability at the Si/SiO$_2$ interface," *Phys. Rev. B, Condens. Matter*, vol. 51, no. 7, pp. 4218–4230, Feb. 1995.

[7] S. Chakravarthi, A. T. Krishnan, V. Reddy, C. F. Machala, and S. Krishnan, "A comprehensive framework for predictive modeling of negative bias temperature instability," in *Proc. IRPS*, 2004, pp. 273–282.

[8] A. T. Krishnan, C. Chancellor, S. Chakravarthi, P. E. Nicollian, V. Reddy, A. Varghese, R. B. Khamankar, and S. Krishnan, "Material dependence of hydrogen diffusion: Implications for NBTI degradation," in *IEDM Tech. Dig.*, 2005, pp. 688–691.

[9] D. Varghese, D. Saha, S. Mahapatra, K. Ahmed, F. Nouri, and M. A. Alam, "On the dispersive versus Arrhenius temperature activation of NBTI time evolution in plasma nitrided gate oxides: Measurements, theory, and implications," in *IEDM Tech. Dig.*, Dec. 2005, pp. 1–4.

[10] C. Shen, M.-F. Li, C. E. Foo, T. Yang, D. M. Huang, A. Yap, G. S. Samudra, and Y.-C. Yeo, "Characterization and physical origin of fast V_{th} transient in NBTI of pMOSFETs with SiON dielectric," in *IEDM Tech. Dig.*, 2006, pp. 333–336.

[11] S. Zafar, "Statistical mechanics based model for negative bias temperature instability induced degradation," *J. Appl. Phys.*, vol. 97, no. 10, pp. 103 709-1–103 709-9, May 2005.

[12] T. Grasser, R. Entner, O. Triebl, H. Enichlmair, and R. Minixhofer, "TCAD modeling of negative bias temperature instability," in *Proc. SISPAD*, Monterey, CA, Sep. 2006, pp. 330–333.

[13] V. Huard, M. Denais, F. Perrier, N. Revil, C. Parthasarathy, A. Bravaix, and E. Vincent, "A thorough investigation of MOSFETs NBTI degradation," *Microelectron. Reliab.*, vol. 45, no. 1, pp. 83–98, Jan. 2005.

[14] T. Yang, C. Shen, M.-F. Li, C. H. Ang, C. X. Zhu, Y.-C. Yeo, G. Samudra, S. C. Rustagi, M. B. Yu, and D.-L. Kwong, "Fast DNBTI components in p-MOSFET with SiON dielectric," *IEEE Electron Device Lett.*, vol. 26, no. 11, pp. 826–828, Nov. 2005.

[15] D. Varghese, S. Mahapatra, and M. A. Alam, "Hole energy dependent interface trap generation in MOSFET Si/SiO$_2$ interface," *IEEE Electron Device Lett.*, vol. 26, no. 8, pp. 572–574, Aug. 2006.

[16] M. Houssa, M. Aoulaiche, S. De Gendt, G. Groeseneken, M. M. Heyns, and A. Stesmans, "Reaction-dispersive proton transport model for negative bias temperature instabilities," *Appl. Phys. Lett.*, vol. 86, no. 9, pp. 093 506-1–093 506-3, Feb. 2005.

[17] B. Kaczer, V. Arkhipov, R. Degraeve, N. Collaert, G. Groeseneken, and M. Goodwin, "Disorder-controlled-kinetics model for negative bias temperature instability and its experimental verification," in *Proc. IRPS*, 2005, pp. 381–387.

[18] L. Tsetseris, X. J. Zhou, D. M. Fleetwood, R. D. Schrimpf, and S. T. Pantelides, "Physical mechanisms of negative-bias temperature instability," *Appl. Phys. Lett.*, vol. 86, no. 14, pp. 142 103-1–142 103-3, Apr. 2005.

[19] J. Kakalios, R. A. Street, and W. B. Jackson, "Stretched-exponential relaxation arising from dispersive diffusion of hydrogen in amorphous silicon," *Phys. Rev. Lett.*, vol. 59, no. 9, pp. 1037–1040, Aug. 1987.

[20] N. H. Nickel, W. B. Jackson, and J. Walker, "Hydrogen migration in polycrystalline silicon," *Phys. Rev. B, Condens. Matter*, vol. 53, no. 12, pp. 7750–7761, Mar. 1996.

[21] F. B. McLean and G. A. Ausman, "Simple approximate solution to continuous-time random-walk transport," *Phys. Rev. B, Condens. Matter*, vol. 15, no. 2, pp. 1052–1061, Jan. 1977.

[22] D. B. Brown and N. S. Saks, "Time dependence of radiation-induced interface trap formation in metal-oxide-semiconductor devices as a function of oxide thickness and applied field," *J. Appl. Phys.*, vol. 70, no. 7, pp. 3734–3747, Oct. 1991.

[23] J. Noolandi, "Multiple-trapping model of anomalous transit-time dispersion in *a*-Se," *Phys. Rev. B, Condens. Matter*, vol. 16, no. 10, pp. 4466–4473, Nov. 1977.

[24] J. Orenstein, M. A. Kastner, and V. Vaninov, "Transient photoconductivity and photo-induced optical absorption in amorphous semiconductors," *Philos. Mag. B, Phys. Condens. Matter Electron. Opt. Magn. Prop.*, vol. 46, no. 1, pp. 23–62, 1982.

[25] V. I. Arkhipov and A. I. Rudenko, "Drift and diffusion in materials with traps," *Philos. Mag. B, Phys. Condens. Matter Electron. Opt. Magn. Prop.*, vol. 45, no. 2, pp. 189–207, 1982.

[26] M. Denais, V. Huard, C. Parthasarathy, G. Ribes, F. Perrier, N. Revil, and A. Bravaix, "Interface trap generation and hole trapping under NBTI and PBTI in advanced CMOS technology with a 2-nm gate oxide," *IEEE Trans. Device Mater. Rel.*, vol. 4, no. 4, pp. 715–722, Dec. 2004.

[27] H. Reisinger, O. Blank, W. Heinrigs, A. Mühlhoff, W. Gustin, and C. Schlünder, "Analysis of NBTI degradation- and recovery-behavior based on ultra fast V_{th}-measurements," in *Proc. IRPS*, 2006, pp. 448–453.

[28] M. Ershov, R. Lindley, S. Saxena, A. Shibkov, S. Minehane, J. Babcock, S. Winters, H. Karbasi, T. Yamashita, P. Clifton, and M. Redford, "Transient effects and characterization methodology of negative bias temperature instability in pMOS transistors," in *Proc. IRPS*, 2003, pp. 606–607.

[29] S. Mahapatra, K. Ahmed, D. Varghese, A. E. Islam, G. Gupta, L. Madhav, D. Saha, and M. A. Alam, "On the physical mechanism of NBTI in

[30] T. Grasser, W. Gös, V. Sverdlov, and B. Kaczer, "The universality of NBTI relaxation and its implications for modeling and characterization," in *Proc. IRPS*, 2007, pp. 268–280.

[31] T. L. Tewksbury and H.-S. Lee, "Characterization, modeling, and minimization of transient threshold voltage shifts in MOSFETs," *IEEE J. Solid-State Circuits*, vol. 29, no. 3, pp. 239–252, Mar. 1994.

[32] J. Ushio, Y. Okuyama, and T. Maruizumi, "Electric-field dependence of negative-bias temperature instability," *J. Appl. Phys.*, vol. 97, no. 8, pp. 1–3, 2005.

[33] C. G. Van De Walle, "Stretched-exponential relaxation modeled without invoking statistical distributions," *Phys. Rev. B, Condens. Matter*, vol. 53, no. 17, pp. 11 292–11 295, May 1996.

[34] N. H. Nickel, A. Yin, and S. J. Fonash, "Influence of hydrogen and oxygen plasma treatments on grain-boundary defects in polycrystalline silicon," *Appl. Phys. Lett.*, vol. 65, no. 24, pp. 3099–3101, 1994.

[35] A. Stesmans, "Dissociation kinetics of hydrogen-passivated P_b defects at the (111)Si/SiO$_2$ interface," *Phys. Rev. B, Condens. Matter*, vol. 61, no. 12, pp. 8393–8403, Mar. 2000.

[36] S. Ogawa, M. Shimaya, and N. Shiono, "Interface-trap generation at ultrathin SiO$_2$ (4 nm–6 nm)-Si interfaces during negative-bias temperature aging," *J. Appl. Phys.*, vol. 77, no. 3, pp. 1137–1148, Feb. 1995.

[37] A. T. Krishnan, S. Chakravarthi, P. Nicollian, V. Reddy, and S. Krishnan, "Negative bias temperature instability mechanism: The role of molecular hydrogen," *Appl. Phys. Lett.*, vol. 88, no. 15, pp. 153 518-1–153 518-3, Apr. 2006.

[38] M. A. Alam, "A critical examination of the mechanics of dynamic NBTI for PMOSFETs," in *IEDM Tech. Dig.*, 2003, pp. 345–348.

[39] J. B. Yang, T. P. Chen, S. S. Tan, and L. Chan, "Analytical reaction–diffusion model and the modeling of nitrogen-enhanced negative bias temperature instability," *Appl. Phys. Lett.*, vol. 88, no. 17, pp. 172 109-1–172 109-3, Apr. 2006.

[40] H. Kufluoglu and M. A. Alam, "Theory of interface-trap-induced NBTI degradation for reduced cross section MOSFETs," *IEEE Trans. Electron. Devices*, vol. 53, no. 5, pp. 1120–1130, May 2006.

[41] M. A. Alam and H. Kufluoglu, "On quasi-saturation of negative bias temperature degradation," *ECS Trans.*, vol. 1, no. 1, pp. 139–145, 2005.

[42] M. A. Alam, "NBTI: A simple view of a complex phenomena," in *Proc. IRPS*, 2006, pp. 191.1–191.22. Tutorial.

[43] J. Crank, *The Mathematics of Diffusion*, 2nd ed. Oxford, U.K.: Clarendon Press, 1975.

[44] M. A. Alam, H. Kufluoglu, D. Varghese, and S. Mahapatra, "A comprehensive model for PMOS NBTI degradation: Recent progress," *Microelectron. Reliab.*, vol. 47, no. 6, pp. 853–862, Jun. 2007.

[45] M. A. Alam, "Negative bias temperature instability: Basics/modeling," in *Proc. IRPS*, 2005, pp. 211.1–211.22. (Tutorial).

[46] S. Zafar, private communications.

[47] H. Scher and E. W. Montroll, "Anomalous transit-time dispersion in amorphous solids," *Phys. Rev. B, Condens. Matter*, vol. 12, no. 6, pp. 2455–2477, Sep. 1975.

[48] V. I. Arkhipov, "Trap-controlled and hopping modes of transport and recombination: Similarities and differences," in *Proc. ISEIM*, 1995, pp. 271–274.

[49] J. Noolandi, "Equivalence of multiple-trapping model and time-dependent random walk," *Phys. Rev. B, Condens. Matter*, vol. 16, no. 10, pp. 4474–4479, Nov. 1977.

[50] F. W. Schmidlin, "Theory of trap-controlled transient photoconduction," *Phys. Rev. B, Condens. Matter*, vol. 16, no. 6, pp. 2362–2385, Sep. 1977.

[51] W. B. Jackson and C. C. Tsai, "Hydrogen transport in amorphous silicon," *Phys. Rev. B, Condens. Matter*, vol. 45, no. 12, pp. 6564–6580, Mar. 1992.

[52] A. I. Rudenko and V. I. Arkhipov, "Drift and diffusion in materials with traps: Quasi-equilibrium transport regime," *Philos. Mag. B, Phys. Condens. Matter Electron. Opt. Magn. Prop.*, vol. 45, no. 2, pp. 177–187, 1982.

[53] V. I. Arkhipov and H. Bässler, "An adiabatic model of dispersive hopping transport," *Philos. Mag. B, Phys. Condens. Matter Electron. Opt. Magn. Prop.*, vol. 68, no. 4, pp. 425–435, 1993.

[54] W. B. Jackson, "Connection between the Meyer-Neldel relation and multiple-trapping transport," *Phys. Rev. B, Condens. Matter*, vol. 38, no. 5, pp. 3595–3598, Aug. 1988.

[55] B. Kaczer, V. Arkhipov, R. Degraeve, N. Collaert, G. Groeseneken, and M. Goodwin, "Temperature dependence of the negative bias temperature instability in the framework of dispersive transport," *Appl. Phys. Lett.*, vol. 86, no. 14, pp. 143 506-1–143 506-3, Apr. 2005.

silicon oxynitride p-MOSFETs: Can differences in insulator processing conditions resolve the interface trap generation versus hole trapping controversy?" in *Proc. IRPS*, 2007, pp. 1–9.

Tibor Grasser (M'05–SM'05) was born in Vienna, Austria, in 1970. He received the Diplomingenieur degree in communications engineering, the Ph.D. degree in technical sciences, and the venia docendi in microelectronics from the Technische Universität Wien, Vienna, in 1995, 1999, and 2002, respectively.

He is currently an Associate Professor at the Institute for Microelectronics, Technische Universität Wien. Since 1997, he has headed the Minimos-NT Development Group, working on the successor of the highly successful MiniMOS program. He was a visiting research engineer with Hitachi Ltd., Tokyo, Japan, and with the Alpha Development Group, Compaq Computer Corporation, Shrewsbury, MA. In 2003, he was appointed as the Head of the Christian Doppler Laboratory for Technology Computer-Aided Design in Microelectronics, an industry-funded research group embedded in the Institute for Microelectronics. He is a coauthor or the author of more than 200 articles in scientific books, journals, and conference proceedings and is the editor of a book on advanced device simulation. His current scientific interests include circuit and device simulation, device modeling, and reliability issues.

Dr. Grasser has been involved in the program committees of conferences such as the International Conference on Simulation of Semiconductor Processes and Devices (SISPAD), the International Workshop on Computational Electronics (IWCE), the European Solid-State Device Research Conference (ESSDERC), the IEEE International Reliability Physics Symposium (IRPS), the International Integrated Reliability Workshop (IIRW), and the International Semiconductor Device Research Symposium (ISDRS). He was also the chairman of SISPAD 2007.

Wolfgang Gös was born in Vienna, Austria, in 1979. He received the Diplomingenieur degree in technical physics, with a thesis on grain boundaries in back contact solar cells, from the Technische Universiät Wien, Vienna, in 2005. He is currently working toward the Ph.D. degree in the Christian Doppler Laboratory for Technology Computer Aided Design, Institute for Microelectronics, Technische Universiät Wien.

He joined the Institute for Microelectronics in January 2006. In 2007, he was a visitor with the Department of Physics and Astronomy, Vanderbilt University, Nashville, TN. His current scientific interests include first-principle simulations of the chemical processes involved in NBTI and HCI, the modeling of tunneling and charge trapping in dielectrics, and reliability issues in general.

Ben Kaczer received the M. S. degree in physical electronics from Charles University, Prague, Czech Republic, in 1992 and the M. S. and Ph.D. degrees in physics from Ohio State University, Columbus, in 1996 and 1998, respectively. For his Ph.D. research on the ballistic-electron emission microscopy of SiO2 and SiC films, he received the OSU Presidential Fellowship and support from Texas Instruments Incorporated.

In 1998, he joined the Reliability Group, Interuniversity Microelectronics Center (IMEC), Leuven, Belgium, where his activities include the research of the degradation phenomena and reliability assessment of SiO2, SiON, high-k, and ferroelectric films, planar and multiple-gate FETs, circuits, and characterization of Ge and GaAs devices. He is the author or a coauthor of more than 100 journal and conference papers.

Dr. Kaczer has served or is serving at various functions at the International Electron Devices Meeting (IEDM), the IEEE International Reliability Physics Symposium (IRPS), the IEEE Semiconductor Interface Specialists Conference (SISC), and the Conference on Insulating Films on Semiconductors (INFOS). He is the recipient of Best and the Outstanding Paper Awards at IRPS.